In silico study to identify novel NEK7 inhibitors from natural source by a combination strategy

Heng Zhang (✉ dg21300053@smail.nju.edu.cn)

Nanjing University

Chenhong Lu (✉ 502022300023@smail.nju.edu.cn)

Nanjing University

QiLong Yao (✉ 522022300047@smail.nju.edu.cn)

Nanjing University

Qingcai Jiao (✉ jiaoqingcai@126.com)

Nanjing University

Additional Declarations: No competing interests reported.

In silico study to identify novel NEK7 inhibitors from natural source by a combination strategy

Heng Zhang [a], Chenhong Lu [a], QiLong Yao [a], Qingcai Jiao [a, *]

[a] State Key Laboratory of Pharmaceutical Biotechnology, School of Life Sciences, Nanjing University, Nanjing, 210023, China
[*] Corresponding author
E-mail addresses: jiaoqingcai@126.com (Q. Jiao).

Abstract

Cancer remains a significant health problem and stands as one of the primary causes of death worldwide. NEK7, a NIMA-related protein kinase, plays a crucial role in spindle assembly and cell division. Dysregulation of the NEK7 protein contributes to the development and progression of various malignancies, such as colon cancer and breast cancer. Therefore, the inhibition of NEK7 shows promise as a potential clinical target for anticancer therapy. Nevertheless, there is a dearth of high-quality NEK7 inhibitors. In this study, we utilized virtual screening, molecular docking, silicon-based pharmacokinetics, molecular dynamics (MD) simulations, and molecular mechanics Poisson-Boltzmann surface area (MM/PBSA)-based binding free energy calculations to comprehensively analyze effective natural inhibitors that target NEK7 within the current framework. By employing molecular docking, including semi-flexible and flexible docking methods, we identified three natural products as hit compounds with binding modes similar to the active control dabrafenib. ADME/T predictions indicated that these hit molecules

exhibited lower toxicity when administered orally. Additionally, through DFT calculations, we determined that the popular compound (-)-balanol possessed high chemical activity. Finally, 100 ns molecular dynamics simulations and energy decomposition revealed that the hit compounds displayed superior binding energy compared to the active control and demonstrated higher affinity. Based on the findings of our current research, we conclude that these newly discovered natural inhibitors may serve as parent structures for the development of more potent derivatives with promising biological activities. However, further experimental validation is necessary as part of subsequent investigations.

Introduction

NIMA-related kinases (NEKs) belong to the family of mitotic kinases, representing the third family of kinases [1]. A notable characteristic of the NEK protein family is the presence of typical serine/threonine kinase motifs in the N-terminal catalytic domain, which exhibits a significant sequence similarity to the *Neurospora crassa* NIMA kinase [2]. NEKs comprise a substantial class of homologous kinases with similar structure and function, participating in various physiological regulatory processes, including mitotic regulation, ciliogenesis, and DNA damage response [3]. Presently, NEKs are found in most eukaryotes, including the human genome, which encompasses 11 genes (NEK1 to NEK11) encoding NEKs [4].

NEK7 is a small member of the NEK kinase family and localizes in the centrosome. It exhibits wide expression in various tissues, including the brain, heart, lungs, liver, and spleen [2]. NEK7 primarily concentrates at the two poles of the spindle, regulating microtubule function and closely contributing to the formation of the mitotic spindle and cytoplasmic separation [5]. Consequently, it plays a crucial role in cell cycle regulation [6]. The NEK7 gene, found on chromosome 1, encodes a polypeptide comprising 34,500 amino acids. NEK7 is predominantly located on both sides of the spindle and consists mostly of catalytic kinase domains, featuring two amino-terminal kinase domains and lacking a carboxyl terminal [7]. Among the NEK family, NEK6 and NEK7 share approximately 86% identity in their C-terminal domains, while their unstructured N-terminal extensions exhibit only about 20% identity. Notably, NEK7, together with NEK6 and NEK9, forms a mitotic signaling module, wherein NEK9 phosphorylates and activates NEK6 and NEK7, collectively promoting mitosis [8]. NEK7 has long been recognized as closely associated with cell division, growth, and the survival of mammalian cells [9].

NEK7, despite its physiological role, exhibits abnormal expression in various tumors, such as retinoblastoma, hepatocellular carcinoma, pancreatic ductal adenocarcinoma, head and neck squamous cell carcinoma, and breast cancer [10-12]. Downregulation of NEK7 levels in numerous cancer cell lines and tumor models has been observed to diminish tumor proliferation, migration, and invasion by influencing the mitotic process [13,14]. These findings indicate the potential of NEK7 as a promising drug target. However, the lack of high-quality NEK7 inhibitors impedes progress in this field. In comparison to conventional drug discovery methods, virtual screening offers a rapid and cost-effective approach

for identifying potential drugs. Moreover, natural products have gained significant global research attention owing to their remarkable chemical diversity and robust biochemical specificity. Consequently, there is a growing focus on exploring potent bioactive compounds derived from herbs and medicinal plants, thus paving the way for multiple pharmacological targets [15-17].

In this study, we conducted the following work to search for novel skeletal natural inhibitors of NEK7. Initially, we performed structure-based virtual screening of a natural compound library to identify compounds that exhibited optimal orientation at the active site of the enzyme and determined their corresponding docking scores. Subsequently, we employed pharmacological models and molecular docking to conduct screening. We utilized ADME/T predictions to explore the pharmacokinetic and pharmacodynamic characteristics of the remaining compounds, with a specific focus on the hit compounds, after docking. Additionally, we conducted density functional theory (DFT) investigations to determine the reaction properties and stability of the positive compounds and natural molecules that showed hits. We utilized DFT calculations to evaluate the HOMO/LUMO analysis, molecular reactivity descriptors, and electrostatic potential (ESP) of the three identified natural products. We performed molecular dynamics simulations (MD) based on the docking scores and binding modes to assess the potential molecular interactions and binding stability within the protein-ligand complexes. Finally, we conducted MM/PBSA binding free energy calculations on the enzyme complex to gain insight into the inhibitor's affinity for the active site.
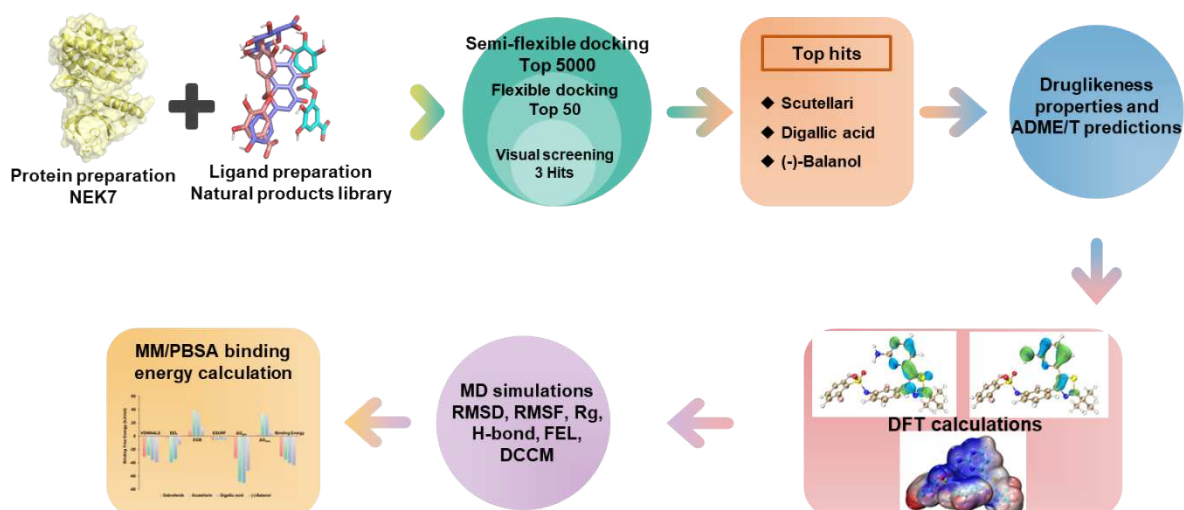
Fig. 1 Overview of the computational workflow implemented for structure-based virtual screening.

Materials and methods

Fig. 1 presents a graphical representation of the structure-based virtual screening (SBVS) workflow used in this study to describe the computational methodology pipeline.

Preparation of ligand

The study evaluated approximately 21,000 compounds extracted from three prominent, large-scale natural product databases globally: InterBioScreen [18] (L6020,19377, accessed via https://www.tsbiochem.com/), The Natural Product Atlas [19,20] (2022_09, 2.3.0, 33372, accessed via https://www.npatlas.org/download), and ZINC [21,22] (160427, accessed via https://www.zinc.docking.org). These natural products were locally stored in Simplified Molecular Input Line Entry System (SDF) format. The obtained two-dimensional compound structures were then transformed into a three-dimensional Protein Data Bank (PDB) format, leveraging the Open Babel tool. Following this, energy minimization of the ligand library was performed using Chem 3D,

employing the Merck Molecular Force Field 94 (MMFF94) and the steepest descent algorithm over 1500 iterations. The ligand library preparation included the addition of gaseous charges to the compounds and rotation of all rotatable bonds, facilitated by AutoDock. The optimized compound library was finally saved in PDBQT format, earmarked for subsequent virtual screening procedures.
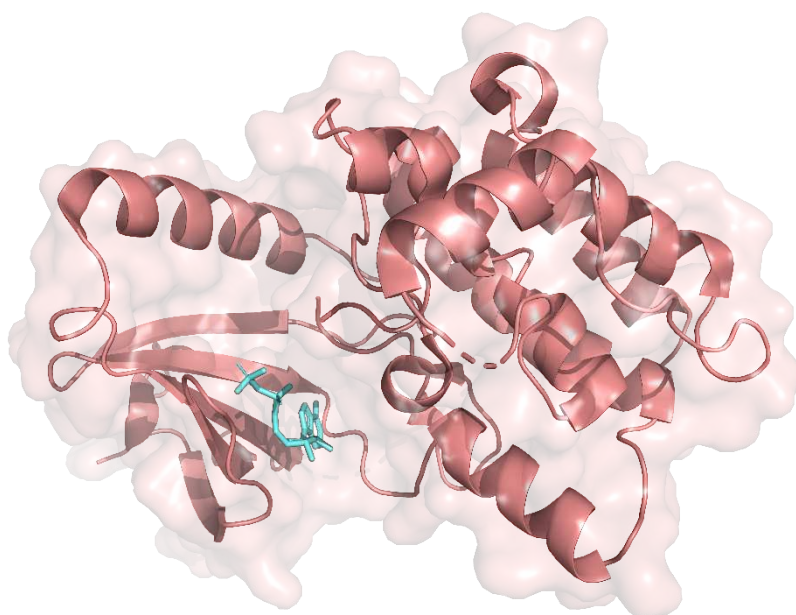

Fig. 2 The 3D structure of NEK7, integrated with ADP (cyan) (PDB ID: 2WQN).

Preparation of protein

A prerequisite for docking experiments is the availability of the protein's three-dimensional structure. The 3D X-ray crystal structure of NIMA-related kinase 7 (NEK7) was retrieved from the Protein Data Bank (PDB ID: 2WQN), exhibiting a resolution of 2.35 Å. Any ligands and heteroatoms, including water molecules, were subsequently removed from this protein. AutoDock v4.2 [23] was then employed for additional protein preparation. The receptor preparation process comprised full hydrogenation, consolidation of

nonpolar hydrogen atoms, and the introduction of Kollman charges [24]. The processed protein is conserved in a local shell for subsequent utilization. The binding site of NEK7 was determined based on the original co-crystal ligand (ADP) (**Fig. 2**).

Re-docking of ligand molecules with receptor targets

Utilizing PyRx software, the NEK7 protein's original ligand was extracted and subsequently redocked into the designated binding pocket of the corresponding target protein, in accordance with pre-established parameters [25]. The appropriateness of these parameters was assessed via the root mean square deviation (RMSD) between the ligand molecule that scored highest post-docking and the co-crystallized ligand molecule. As a general rule, an RMSD of ≤ 2 Å [26] indicates a successful replication of the initial binding mode between ligand and receptor through the docking procedure, thereby affirming the reasonableness of the docking parameters.

Molecular docking

Molecular docking is a technique designed to identify the optimal binding mode via the synergistic effect of energy matching, geometric complementarity, and chemical environment compatibility between a ligand and the active pocket [27]. In this study, we utilized this method to ascertain the binding orientation of various natural products within the active pocket of the NEK7 protein. Using the Vina software, we conducted a virtual screening of natural product datasets. In this context, the Lamarckian Genetic Algorithm of ADT (AutoDock's graphical user interface) was employed to explore active binding spaces of varying efficacies. The binding site of MAO-A had been predefined due to the co-

crystallization of the MLG ligand with FAD. We defined the grid box in the receptor region bound by MLG, enabling the ligand library to identify a feasible docking location [28]. The parameters for the grid center were set at 37.0, 37.01, and 47.42, while the docking box dimensions were 20×20×20 Å^3. For virtual screening, we performed 250 Lamarckian GA runs, yielding a maximum of 27,000 generations and 250,000 evaluations. We initially applied semi-flexible docking to 21,376 molecules, subsequently progressing the top-ranked molecules (characterized by a potent binding force and high docking score at the NEK7 active site) to a flexible docking mode. In the end, we saved the best pose for each molecule during the docking process. Given its proven efficacy as an inhibitor of the NEK9 protein, and the structural similarity between NEK7 and NEK9, dabrafenib was also incorporated into the docking analysis as a reference compound, alongside selected popular molecules [29].

Density functional theory calculations

Density Functional Theory (DFT) serves as a robust and efficacious method for the precise estimation of a compound's electronic properties [30]. Using the Lee-Yang-Parr correlation function (B3LYP) theory and a 6-31G**++ basis set, we optimized natural compounds identified as hit compounds. This optimization sought to enhance the binding affinity of these natural compounds with NEK7 [30]. This study utilized Gaussian 09W software for the optimization and frequency computations of the chosen drugs. The Gaussian View 6 program facilitated the visualization of HOMO/LUMO orbitals and the structures' optimization. All computations employed the SVP basis set. The optimized compounds underwent calculations to determine electronic properties, such as HOMO (Highest Occupied Molecular Orbital), LUMO (Lowest

Unoccupied Molecular Orbital), and Molecular Electrostatic Potential (MESP). The regions of electron donors and acceptors in the hit compounds were identified through HOMO and LUMO [31]. The energy gap between HOMO and LUMO dictated the chemical stability and biological activity characteristics of the hit molecules [32]. The electrostatic potential and spatial diffusion (moving away from the molecular surface) of the identified compound's van der Waals contact surface were critical for measuring charge distribution from an emergent reagents' perspective. The colored isosurface values symbolize the overall molecular size and positive electrostatic potential. The compound's regions with the highest and lowest electrostatic potentials are dyed deepest blue and deepest red, respectively. DFT was employed to collect molecular geometric parameters, frontier molecular orbitals (FMO), global and local reactivity descriptors, and molecular electrostatic potential (MEP). Mathematical formulas facilitated the following computations [33]:

$$\Delta E^{\text{gap}} = E^{\text{LUMO}} - E^{\text{HOMO}}$$

$$\text{Electron affinity (EA)} \approx -(\text{LUMO})$$

$$\text{Ionization potential (IP)} \approx -(\text{HOMO})$$

$$\text{Hardness } (\eta) \approx \frac{\text{IP} - \text{EA}}{2}$$

$$\text{Softness } (\sigma) \approx \frac{1}{2\eta}$$

$$\text{Electronegativity } (\chi) \approx \frac{\text{IP} + \text{EA}}{2}$$

$$\text{Chemical potential } (\mu) \approx -\chi$$

$$\text{Electrophilicity index } (\omega) \approx \frac{\mu^2}{2\eta}$$

In silico drug-likeliness and ADME/T prediction

ADME/T (Absorption, Distribution, Metabolism, Excretion, and Toxicity) properties of compounds play a crucial role in drug design and screening [34]. An early assessment of these properties can effectively address interspecies variations, thereby enhancing drug development success rates, reducing development costs, minimizing drug toxicity, and informing appropriate clinical use [35]. This study investigates the physicochemical properties (ADME traits) of potential natural molecules to identify key parameters impacting biological activity. To predict the drug-like properties and pharmacokinetics/toxicity of both control compounds and identified natural product molecules, we utilize the ADMETlab 2.0 server (https://admetmesh.scbdd.com) [36].

Molecular dynamics simulation (MDs)

To delve into the binding stability of prominent compounds yielded from virtual screening and proteins within the experimental milieu, a molecular dynamics simulation, spanning 100 nanoseconds, was executed on the complex post-molecular docking. All simulations were executed employing the GROMACS software package (v.2018.8) [37], with the charmm36 force field [38] designated for the protein. Preparation of the protein topology file was accomplished through the pdb2gmx tool [39], while the Automated Topology Builder (ATB v3.0) [40] generated the ligand ITP file with the gro-mos54a71 force field. The complex was confined within a cube of 1nm border size, the exterior of the protein-ligand region filled with the SPC water model. In an effort to conserve the system's electrical neutrality, a proportion of water molecules were supplanted with sodium and chloride ions, thus fashioning a solvent box with 0.15 mol/L NaCl. Initially, energy minimization of the system was achieved using the steepest descent method, ensuring

the absence of geometric conflicts or inappropriateness. Following this, equilibrium was established for each system's NVT and NPT. Over a 100 picoseconds equilibrium period, the atom count, volume, and temperature were maintained within the NVT ensemble. Thereafter, the system persisted in establishing equilibrium for another 100 picoseconds in the NPT ensemble, maintaining constant atom count, pressure, and temperature. With a step size of 2.0 femtoseconds, the system underwent a 100 nanoseconds molecular dynamics simulation at 300 Kelvin and one atmosphere. Analysis was conducted on root mean square displacement (RMSD), root mean square fluctuation (RMSF), radius of gyration (Rg), and hydrogen bonds, founded on the MD simulation trajectory.

MM/PBSA binding free energy calculations

Binding energy calculations are highly beneficial during the advanced phases of drug discovery [41]. This study employed the Molecular Mechanics Poisson-Boltzmann Surface Area (MM/PBSA) [42] approach to calculate the binding free energy of the complex created by NEK7 and the identified natural product. The binding free energy computation utilized the gmx_MMPBSA program (https://github.com/Valdes-Tresanco-MS/gmx_MMPBSA) [43]. Our methodology incorporated the complete Molecular Dynamics (MD) trajectory of the protein-ligand complex, capturing snapshots at 200-picosecond intervals. These snapshots facilitated the analysis of binding free energy and identification of protein residues that contribute to the complex's binding free energy.

$$\Delta G^{bind} = \Delta G^{gas} + \Delta G^{solv} = E^{VDWAALS} + E^{EL} + E^{PB} + E^{SURE}$$

$$\Delta G^{gas} = E^{VDWAALS} + E^{EL}$$

$$\Delta G^{solv} = E^{PB} + E^{SURE}$$

ΔG_{bind} is the binding free energy; ΔG_{gas} is the total gas phase free energy; ΔG_{solv} is the total solvation free energy; $E_{VDWAALS}$ is the van der Waals energy; E_{EL} is the electrostatic energy; E_{PB} is the polar solvation energy; E_{SURE} is the non-polar solvation energy.

Results and discussion

Re-docking results of ligand molecules with receptor targets

Before initiating large-scale virtual screening, the validity of parameter settings should be assessed using the RMSD values, derived from the comparison of docked ligand molecules with their original counterparts. An RMSD value equal to or less than 2 Å signifies the reasonableness of the docking parameter settings, reflecting a high overlap between the docked and original ligand molecules [26]. This correlation implies that a higher overlap corresponds to a smaller RMSD value. The redocked ligand aligns significantly with the original ligand, evidenced by the RMSD value of 0.164 Å for ADP (refer to Supporting Information **Fig. S1**). Such an observation substantiates the reliability of the chosen docking methodology.

Structure-based virtual screening (SBVS) of natural products

A comprehensive search for novel chemical types was performed through several screening rounds, which resulted in the selection of three natural compounds out of a total of 213,176 compounds. These compounds were derived from three different natural product databases: InterBioScreen, The Natural Product Atlas, and ZINC. Given the functional and structural similarities between NEK7 and NEK9, we used Dabrafenib, a potent NEK9 inhibitor (with an IC_{50} value of 1–9 nM), as an active reference compound. The docking

score of Dabrafenib with NEK7 served as the benchmark for our virtual screening process. Natural products from the databases mentioned underwent two rounds of docking with varying precision levels, namely semi-flexible docking and flexible docking, to ascertain their potential affinity with NEK7. From the semi-flexible docking process, we identified 56,375 compounds that exhibited higher affinity with NEK7, surpassing the -8.909 kcal/mol docking score of Dabrafenib with NEK7. Additionally, the top 5,000 compounds, which demonstrated binding energies ranging from -12.0 to -17.0 kcal/mol, were classified as high-ranking compounds. These compounds potentially showcase a more potent inhibitory impact on NEK7.

In the subsequent analysis, several amino acids located on NEK7's active loop, specifically Ala61, Ala165, Asp118, Gly117, Ala116, Arg121, Lys63, Gly43al48, Gly41, Leu111, Leu113, Phe168, Asp115, Ala114, Asp179, Ile40, Asn166, and Ile40, were identified for their flexibility, which aids in the docking of high-ranking compounds with NEK7. Three natural product molecules, namely, scutellarin, digallic acid, and (-)-balanol, were singled out for their high NEK7 affinity and multiple interactions. These selections were made based on docking score rankings and visual screening, with docking scores of -11.547, -13.059, and -15.054 kcal/mol, respectively. In comparison, the flexible docking score of dabrafenib, the active control compound, with NEK7 was -9.071 kcal/mol. The molecular structures of the SBVS shortlisted compounds, along with their docking scores and interacting residues, are detailed in **Table 1** and **Fig. 3**. An in-depth interaction analysis will be presented in the following section.

Examining their structure, the natural products that bind tightly to NEK7 are structurally diverse, and the three aforementioned

molecules have unique skeletal configurations. Of particular note, recent research has found scutellarin to influence genes associated with tumor cell proliferation, migration, angiogenesis, and metabolism via the regulation of cellular signaling pathways. Moreover, scutellarin alters the tumor microenvironment to promote an enhanced immune cell response and curb excessive inflammation, a mechanism leveraged by tumor cells for their growth [44]. Digallic acid, a polyphenolic compound isolated from *Pistacia lentiscus* L. fruits, selectively triggers apoptosis in cancer cells [45,46]. Furthermore, (-)-Balanol, a natural product originally isolated from Verticillium balanoides, mimics ATP and inhibits protein kinase C (PKC) isozymes and cAMP-dependent protein kinase (PKA) with minor selectivity. The frequent implication of PKCε in cancer progression suggests its potential as an anticancer drug target [47]. Given the established activities of these compounds, they show promise for cancer chemotherapy. With the support of NEK7-based virtual screening results, we propose that they may contribute to anticancer activities by acting on NEK7.

Table 1 The complete detail of shortlisted compounds.

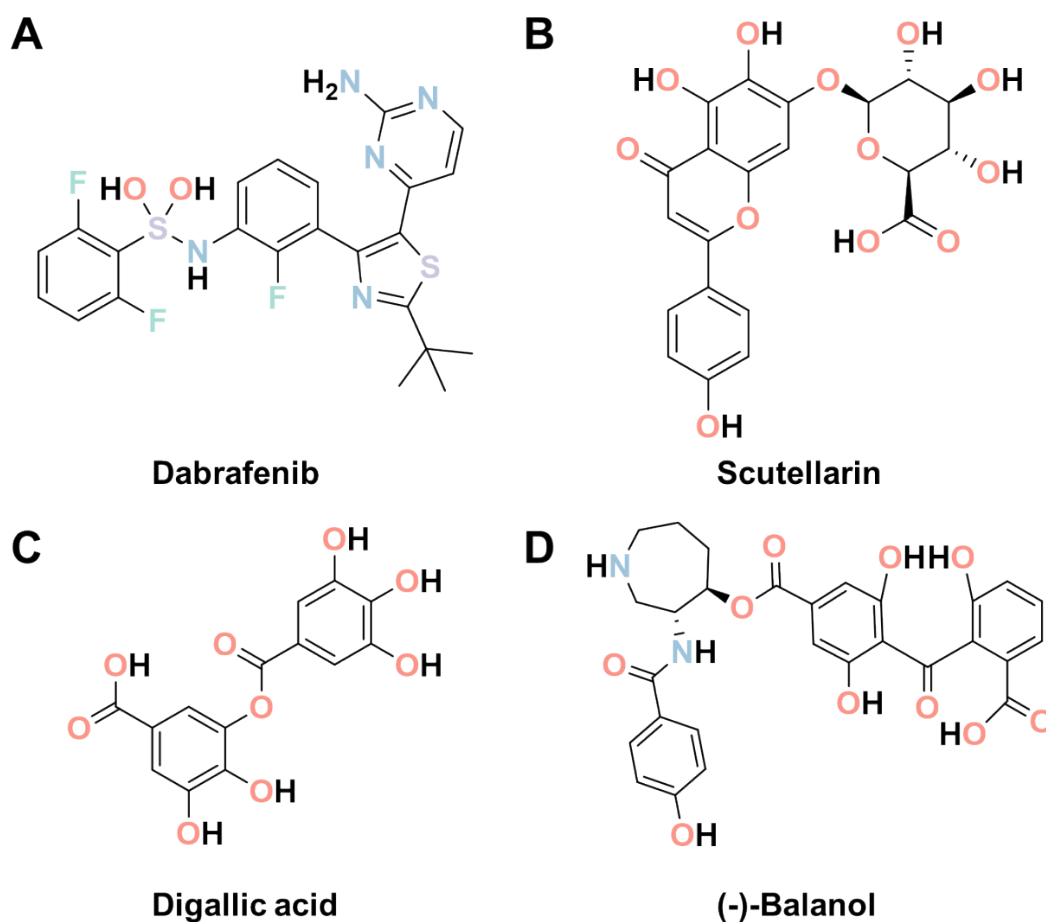| PubChem CID	Molecular Formula	Compounds Names	Molecular Weight	Origin Organism	Origin Genus	Origin Species
185617	$C_{21}H_{18}O_{12}$	Scutellarin	462.4	Plant	*Erigeron*	*breviscapus*
341	$C_{14}H_{10}O_9$	Digallic acid	322.22	Plant	*Pistascia*	*lentiscus*
5287736	$C_{28}H_{26}N_2O_{10}$	(-)-Balanol	550.5	Fungus	*Verticillium*	*balanolides*

Fig. 3 The two-dimensional (2D) chemical structures of reference (A) and top-hit (B-D) molecules shortlisted from SBVS against NEK7.

3.3. Molecular docking analysis of candidate molecules

To uncover the binding potential and mode of action of the shortlisted natural products with NEK7, we evaluated an interaction analysis of their molecular docking. This evaluation aimed to improve our understanding of their pharmacological activity and binding mechanism against NEK7. In these studies, each ligand demonstrated several binding interactions with the receptor (**Table 2**). The docking order, based on scores, was as follows: (-)-balanol > digallic acid > scutellarin.

First, we observed the binding mode of dabrafenib with NEK7's active pocket (docking score=-9.071 kcal/mol). Dabrafenib primarily bound to the catalytic loop, interacting with several key amino acids (**Fig. 4A**). The 2-aminopyrimidine ring of dabrafenib formed a hydrogen bond with GLU112, which partially represents the strength of the bond. Another hydrogen bond was detected between the benzene sulfonamide fragment and Ile40. Additionally, certain nonpolar amino acids in the catalytic loop, such as Ile40, Phe45, Val48, formed hydrophobic interactions with dabrafenib.
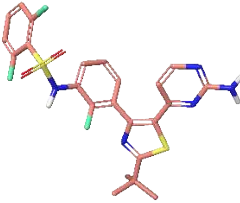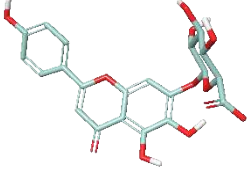
Next, the docking conformation of scutellarin with NEK7's active pocket resulted in a stable protein-ligand complex (docking score -11.547 kcal/mol). Scutellarin exhibited significant molecular interactions, such as hydrogen bonds and hydrophobic interactions, due to its polyhydroxy and polycyclic structure. These interactions stabilize the protein-ligand complex. The glucose part of scutellarin formed hydrogen bonds with Gln44, Ser46, Asp179, and Leu180. Furthermore, the phenolic hydroxyl of the flavone part also formed hydrogen bond interactions with Glu112 and Ala114, allowing scutellarin better NEK7 binding ability than Dabrafenib (**Fig. 4B**).
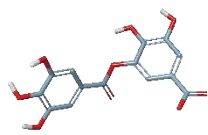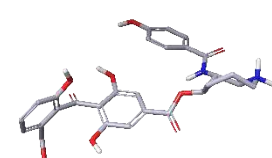
The docking conformation of digallic acid revealed strong hydrophobic and hydrophilic interactions with the active site amino acid residues (**Fig. 5A**). Digallic acid forms six hydrogen bonds with various amino acids in the active site, all related to the hydroxyl groups on the benzene ring. However, in comparison to scutellarin, digallic acid had fewer hydrophobic interactions with the active loop.

Finally, the molecular interactions of (-)-Balanol involved crucial amino acid residues in the target protein's active pocket. (-)-Balanol exhibited significant molecular interactions that contribute to the binding affinity and binding score of the protein-ligand complex. Unlike dabrafenib, (-)-Balanol has more hydrophilic interactions and

fewer hydrophobic interactions. These interactions significantly enhance the binding energy. **Fig. 5B** presents the potential two-dimensional and three-dimensional binding mechanisms of (-)-Balanol.

Table 2 Comprehensive molecular docking results of the reference dabrafenib and top-hit natural compounds.

Compound name	Structure	Semi-flexible docking score	Flexible docking score	Interacting residues	H-bond	H-bond number
Dabrafenib		-8.909	-9.071	Lys38, Ile40, Gly41, Arg42, Gly43, Ser46, Val48, Ala61, Ile95, Leu111, Glu112, Leu113, Ala114, Asp115, Gly117, Arg121, Phe168, and Asp179	**ILE40, GLU112**	2
Scutellarin		-10.016	-11.547	Ile40, Gly41, Arg42, Gly43, Gln44, Phe45, Ser46,	**GLN44, SER46, GLU112, ALA1**	6

				Val48, Ala61, Lys63, Ile95, Leu111, Glu112, Leu113, Ala114, Asp115, Lys163, Phe168, Asp179, Leu 180, and Thr199	**14, ASP1 79, LEU1 80**	
Digallic acid		-11.68 4	-13.05 9	Ile40, Val48, Ala61, Ile95, Leu111, Glu112, Leu113, Ala114, Asp115, Lys163, Asn166, Phe168, Gly178, Asp179, Leu 180, and Thr199	**GLU1 12, ALA1 14, LYS1 63, ASN1 66, ASP1 79**	6
(-)- Balanol		-12.31 9	-15.05 4	Ile40, Gly41, Arg42, Gly43, Gln44, Phe45, Ser46, Val48, Ala61, Lys63,	**PHE4 5, SER4 6, ALA1 14, ASP1 15, ASP1 79**	7

Ile95,
Leu111,
Glu112,
Leu113,
Ala114,
Asp115,
Gly117,
Asp118,
Arg121,
Lys163,
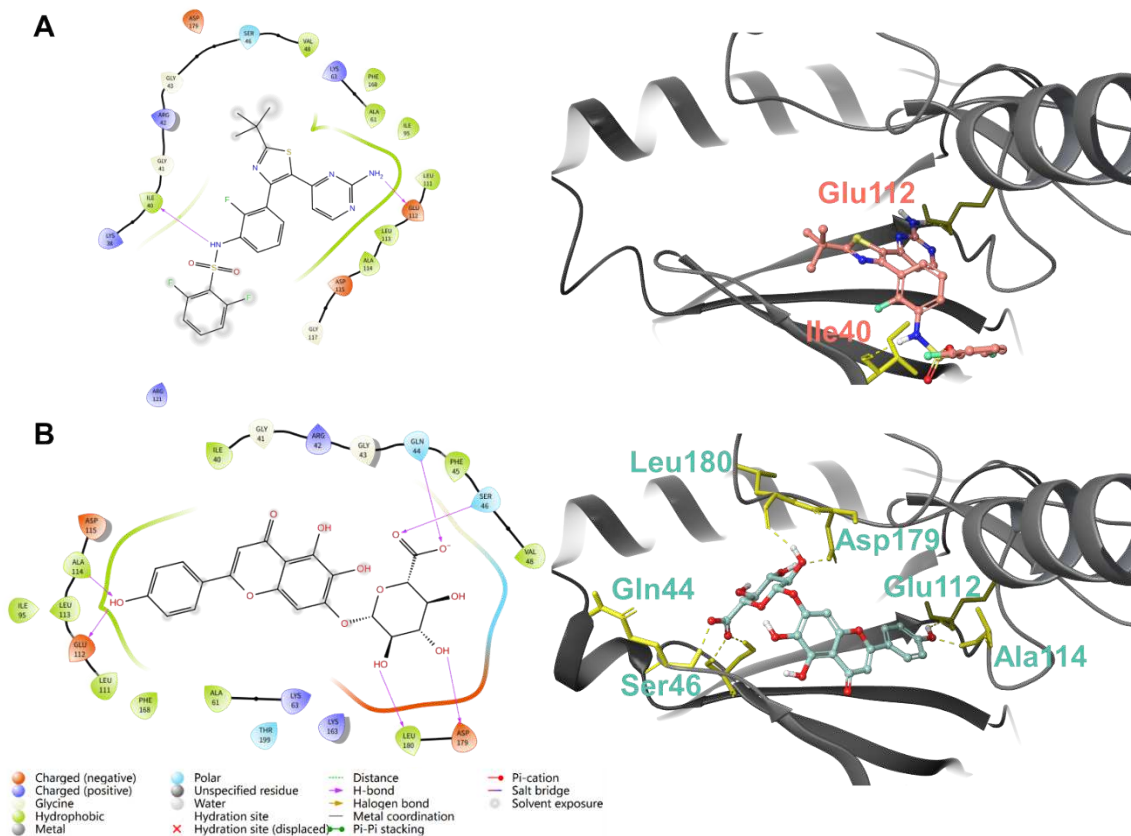Phe168,
Gly178,
Asp179,
Leu
180,
and
Thr199

Fig. 4 2D and 3D docking results of **(A)** dabrafenib and **(B)** scutellarin with NEK7. Hydrogen bonds were shown in yellow.
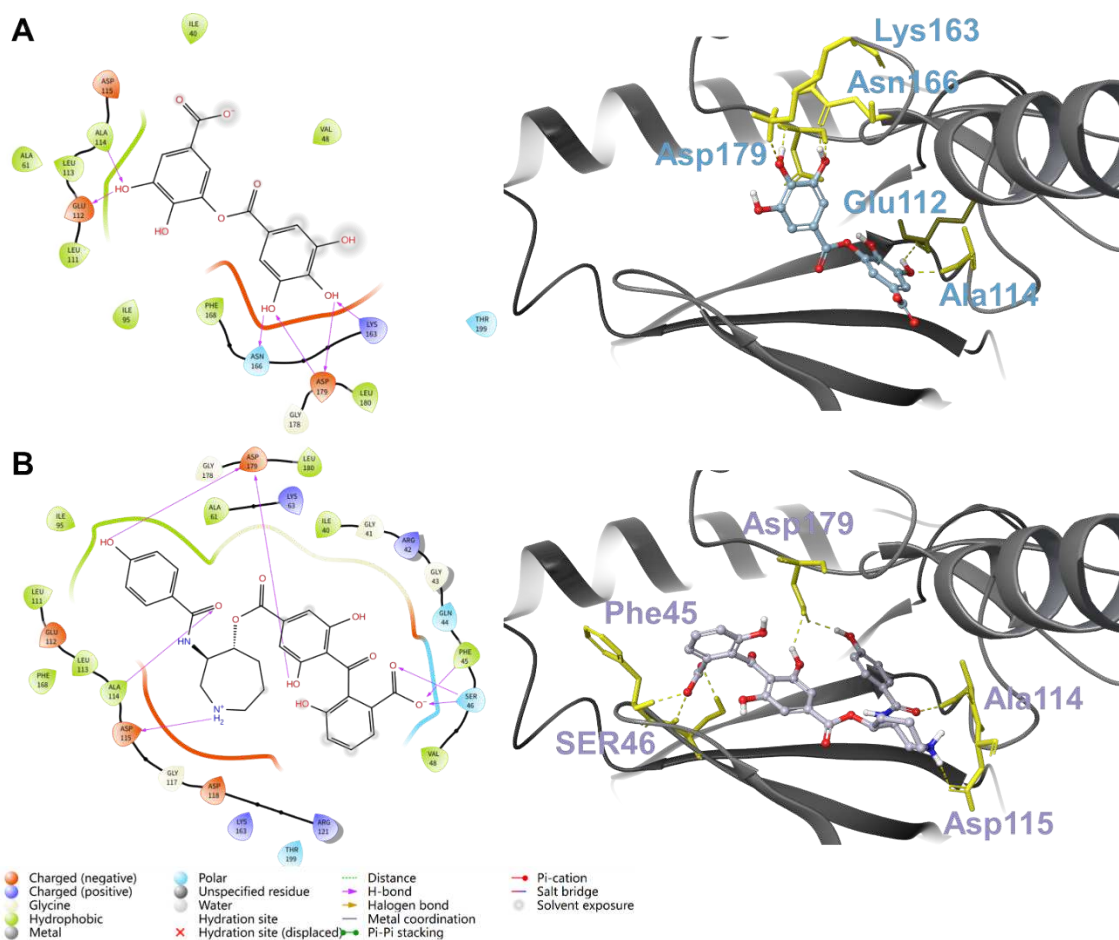
Fig. 5 2D and 3D docking results of **(A)** digallic acid and **(B)** (-)-balanol with NEK7. Hydrogen bonds were shown in yellow.

ADME/T predictions of the hit compounds selected from virtual screening

Table 3 Predicted physiochemical and druglikeness properties of the reference dabrafenib and top-hit natural compounds.

Molecular property	Dabrafenib	Scutellarin	Digallic acid	(-)-Balanol
nHA [a]	7	12	9	12
nHD [b]	3	7	6	7
nRot [c]	6	4	4	9
TPSA [d]	111.59	207.35	164.75	202.72
Molecular Weight	519.1	462.08	322.03	550.16
logP [e]	4.15	0.751	1.352	3.253

Lipinski rule[f]	Accepted	Rejected	Accepted	Rejected

[a] Number of hydrogen bond acceptors. [b] Number of hydrogen bond donors. [c] Number of rotatable bonds. [d] Topological polar surface area. [e] Log of the octanol/water partition coefficient. [f] If two properties are out of range, a poor absorption or permeability is possible, one is acceptable.

The physicochemical attributes of prospective compounds are pivotal parameters closely associated with the preliminary phase of drug discovery. A molecule's likelihood of being a successful drug (drug-likeness) frequently hinges on these characteristics. **Table 3** presents the physicochemical profiles of the natural product candidates and active compounds. The Lipinski's Rule of Five, a guideline for identifying potential orally bioavailable drugs, sets forth the following criteria: molecular weight below 500 Da, fewer than five hydrogen bond donors, fewer than ten hydrogen bond acceptors, and a calculated logP (octanol-water partition coefficient) below 5 [48]. Dabrafenib and digallic acid comply with Lipinski's Rule, but scutellarin and (-)-balanol exceed its thresholds. In detail, scutellarin infringes upon the rule regarding the count of hydrogen bond donors and acceptors, and (-)-balanol breaches the restrictions on molecular weight and hydrogen bond donors and acceptors, likely attributable to the preponderance of hydroxyl groups within their molecular structures. This suggests potential absorption or permeation issues. Notwithstanding, the logP values of all candidate compounds, including dabrafenib, reside within acceptable limits, suggesting an optimal equilibrium between permeability and first-pass elimination. The total polar surface area and quantity of rotatable bonds can dictate a molecule's passive transport, enabling the prediction of the drug's transport attributes [49]. Except for

dabrafenib, the total polar surface areas of most compounds exceed 140 $Å^2$ [50], indicating potential challenges in absorption and transport for these candidate compounds.

Table 4 Predicted ADME properties of the reference dabrafenib and top-hit natural compounds.

Parameter	Dabrafenib	Scutellarin	Digallic acid	(-)-Balanol
Absorption				
Caco-2 permeability [a]	-5.816	-6.389	-6.063	-6.462
MDCK permeability [b]	$8.7e^{-5}$	$1.2e^{-5}$	$5e^{-6}$	$5e^{-6}$
Pgp-inhibitor [c]	0.973	0	0.002	0.003
Pgp-substrate [d]	0.001	0.544	0.009	0.424
Distribution				
PPB [e]	100.6 %	91.38 %	90.72 %	95.67 %
VD [f]	0.509	0.662	0.524	0.961
Metabolism [g]				
CYP1A2 inhibitor	0.339	0.054	0.053	0.538
CYP1A2 substrate	0.350	0.032	0.036	0.034
CYP2C19 inhibitor	0.908	0.029	0.017	0.115
CYP2C19 substrate	0.061	0.045	0.029	0.032
CYP2C9 inhibitor	0.917	0.013	0.47	0.583
CYP2C9 substrate	0.097	0.207	0.036	0.056
CYP2D6 inhibitor	0.848	0.016	0.012	0.120
CYP2D6 substrate	0.085	0.134	0.090	0.115
CYP3A4 inhibitor	0.885	0.014	0.030	0.191
CYP3A4 substrate	0.863	0.003	0.013	0.088
Excretion				
CL [h]	1.55	1.267	8.182	1.988
$T_{1/2}$ [i]	0.237	0.921	0.97	0.862

[a] Optimal: higher than -5.15 Log unit. [b] Low permeability: < 2 × 10^{-6} cm/s. Medium permeability: 2-20 × 10^{-6} cm/s. High passive

permeability: $> 20 \times 10^{-6}$ cm/s. [c] Category 1: inhibitor; Category 0: non-inhibitor. The output value is the probability of being Pgp-inhibitor. [d] Category 1: substrate; Category 0: non-substrate. The output value is the probability of being Pgp-substrate. [e] Plasma protein binding. Optimal: < 90 %. Drugs with high protein-bound may have a low therapeutic index. [f] Volume distribution. Optimal: 0.04-20 L/kg. [g] Category 1: inhibitor or substrate; Category 0: non-inhibitor or non-substrate. The output value is the probability of being inhibitor or substrate. [h] Clearance. High: > 15 mL/min/kg; moderate: 5-15 mL/min/kg; low: < 5 mL/min/kg. [i] Category 1: long half-life; Category 0: short half-life. long half-life: > 3 h; short half-life: < 3 h. The output value is the probability of having long half-life.

Table 5 Predicted toxicity properties of the reference dabrafenib and top-hit natural compounds.

Molecular property	Dabrafenib	Scutellarin	Digallic acid	(-)-Balanol
hERG blockers [a]	0.345	0.149	0.015	0.370
H-HT [b]	0.997	0.138	0.407	0.139
DILI [c]	0.994	0.975	0.811	0.986
Skin sensitization [d]	0.051	0.346	0.931	0.084
Carcinogen city [e]	0.17	0.092	0.018	0.066
Eye corrosion [f]	0.003	0.003	0.058	0.003
Eye irritation [g]	0.008	0.076	0.907	0.011

[a] Category 1: active; Category 0: inactive; The output value is the probability of being active. [b] Human hepatotoxicity. Category 1: H-HT positive (+); Category 0: H-HT negative (-); The output value is the probability of being toxic. [c] Drug induced liver injury. Category 1: drugs with a high risk of DILI; Category 0: drugs with no risk of

DILI. The output value is the probability of being toxic. **d** Category 1: sensitizer; Category 0: non-sensitizer; The output value is the probability of being sensitizer. **e** Category 1: carcinogens; Category 0: non-carcinogens; The output value is the probability of being toxic. **f** Category 1: corrosives; Category 0: non-corrosives; The output value is the probability of being corrosives. **g** Category 1: irritants; Category 0: non-irritants; The output value is the probability of being irritants.

An ideal drug candidate should meet ADME and toxicology standards, reflected by acceptable molecular descriptor values [51,52]. Employing the SBVS method, we identified certain hit molecules and evaluated their pharmacokinetic properties. We used ADMETlab2.0, an online tool, to compute the pharmacokinetic properties of three candidate compounds and dabrafenib, the results of which are presented in **Table 4**. The predicted permeability of the Caco-2 cell line, a model of human colon carcinoma, seems to mirror the intestinal absorption capacity of the ligand. Our observations revealed that all hit and positive compounds exhibited Caco-2 permeability values below 5.15, suggesting that these compounds may not be suitable for oral administration without modification to mitigate adverse properties. Regarding Madin-Darby Canine Kidney (MDCK) permeability, all candidate natural products fall within the recommended range, implying some permeability despite sub-optimal absorption. Furthermore, although high Plasma Protein Binding (PPB) can interfere with drug bioavailability, it may also prolong a drug's half-life, and vice versa. The PPB values of these potential compounds exceeded the recommended range, implying possible bioavailability interference but potential half-life enhancement, a hypothesis supported by the clearance (CL) and

half-life (T1/2) predictions. The drug reaches other body parts via bloodstream circulation, followed by hepatic metabolism [53]. A set of cytochrome P450 family enzymes can metabolize and expel these compounds from the body as bile and urine. Certain bioactive substances serve as substrates for these enzymes, undergoing metabolism by the corresponding CYP450 enzymes [54]. In contrast, some bioactive substances inhibit these enzymes, disrupting the biodegradation process. The results highlight that the active compounds inhibit CYP2C19, CYP2C9, CYP2D6, and CYP3A4. Scutellarin, a natural product, may show affinity for CYP2C9; Digallic acid could be a CYP2C9 inhibitor; and (-)-Balanol might antagonize both CYP1A2 and CYP2C9.

The potential toxicities of active and candidate compounds, displayed in **Table 5**, identify a shared risk of potential drug-induced liver injury. In addition, scutellarin displayed moderate skin sensitization, digallic acid exhibited moderate human hepatotoxicity alongside notable skin sensitization and eye irritation, and (-)-Balanol is a mild Herg blocker. These findings suggest oral administration might be the least toxic method, subject to further experimental verification.

Table 6 FMOs energetic parameters for the reference dabrafenib and top-hit natural compounds in water phase.

Compound	E_{HOMO} (eV)	E_{LUMO} (eV)	ΔE_{gap} (eV)	Potential ionization I (eV)	Electron affinity A (eV)
Dabrafenib	-0.222	-0.062	0.161	0.222	0.062
Scutellarin	-0.212	-0.063	0.149	0.212	0.063
Digallic acid	-0.220	-0.051	0.169	0.220	0.051
(-)-Balanol	-0.221	-0.074	0.147	0.221	0.074

Table 7 Global reactivity descriptors for the reference dabrafenib and top-hit natural compounds in water phase.

Compound	Hardness (η)	Softness (σ)	Electronegativity (χ)	Chemical potential (μ)	Electrophilicity index (ω)
Dabrafenib	0.080	6.22	0.142	-0.142	0.125
Scutellarin	0.074	6.72	0.138	-0.138	0.127
Digallic acid	0.085	5.91	0.135	-0.135	0.108
(-)-Balanol	0.074	6.80	0.148	-0.148	0.148

Frontier molecular orbital analysis (FMO)

High-ranking natural product molecules and the reference compound, dabrafenib, were analyzed using frontier molecular orbital methods to delineate key electronic properties [55], inclusive of molecular geometry optimization, HOMO/LUMO analysis, electrostatic potential, frontier molecular orbital energy, energy parameters, and global reactivity descriptors. Frontier Molecular Orbitals (FMOs), specifically HOMO and LUMO, elucidate the molecular characteristics and reactivity in theoretical chemistry. HOMO and LUMO represent a compound's capacity to donate and accept or withdraw electrons, respectively. These factors critically influence the compound's chemical stability. The band gap, computed by juxtaposing the HOMO and LUMO states of a compound, serves to ascertain its chemical reactivity and kinetic stability. A smaller gap corresponds to elevated compound reactivity [56]. All compounds, except for digallic acid (ΔE_{gap}=0.169 eV), demonstrated smaller bandgap values than dabrafenib, suggestive of their molecular reactivity. This reactivity potentially results in

potent and stable interactions with the NEK7 protein. The HOMO and LUMO sites were plotted on the molecular surface orbitals, thereby determining the molecule's acceptability. **Fig. 6** exhibits the HOMO and LUMO maps (blue for the positive phase, red for the negative phase) of dabrafenib and three natural product molecules.

Additional insight into the reactivity and stability of compounds arises from factors like electronegativity, ionization potential, electron affinity, hardness, and softness [57]. **Table 6** displays the collective reactivity descriptors of both drugs. Chemical hardness and softness also govern a molecule's stability and chemical reactivity. Natural products, scutellarin, and (-)-balanol, are likely to be more susceptible to chemical reactions or interactions due to their chemical softness and hardness ranking (**Table 7**). Electronegativity characterizes a compound's electron acceptance capability, while the electrophilic index (omega) quantifies the affinity of electron acceptors for additional charges from the environment. The natural compound (-)-balanol exhibits the highest electronegativity and electrophilic index, signifying its potential as a superior electron acceptor.

Additionally, the MEP of these four compounds was calculated to discern and explore the stereo-electronic complementarity between the ligand and its receptor, an essential feature for molecular recognition in protein-ligand interactions. It highlights the most electrophilic (susceptible to nucleophilic attack) and electronegative (prone to electrophilic attack) sites. These sites incorporate data about atoms capable of non-covalent interactions within the compound. **Fig. 7** illustrates the molecular electrostatic potentials of the three natural products and dabrafenib, with the compounds' surface MEP values denoted by gradient colors. Red, blue, and gray correspond to areas with the highest electronegative

(electrophilic attack-prone), electropositive (nucleophilic attack-prone), and zero electrostatic potential, respectively. The electrostatic potential contour maps of the compounds reveal potential sites for electrophilic and nucleophilic attacks. Predominantly, the blue sites are located in the carbonyl region, while the red sites cluster within hydroxyl or amino structures.
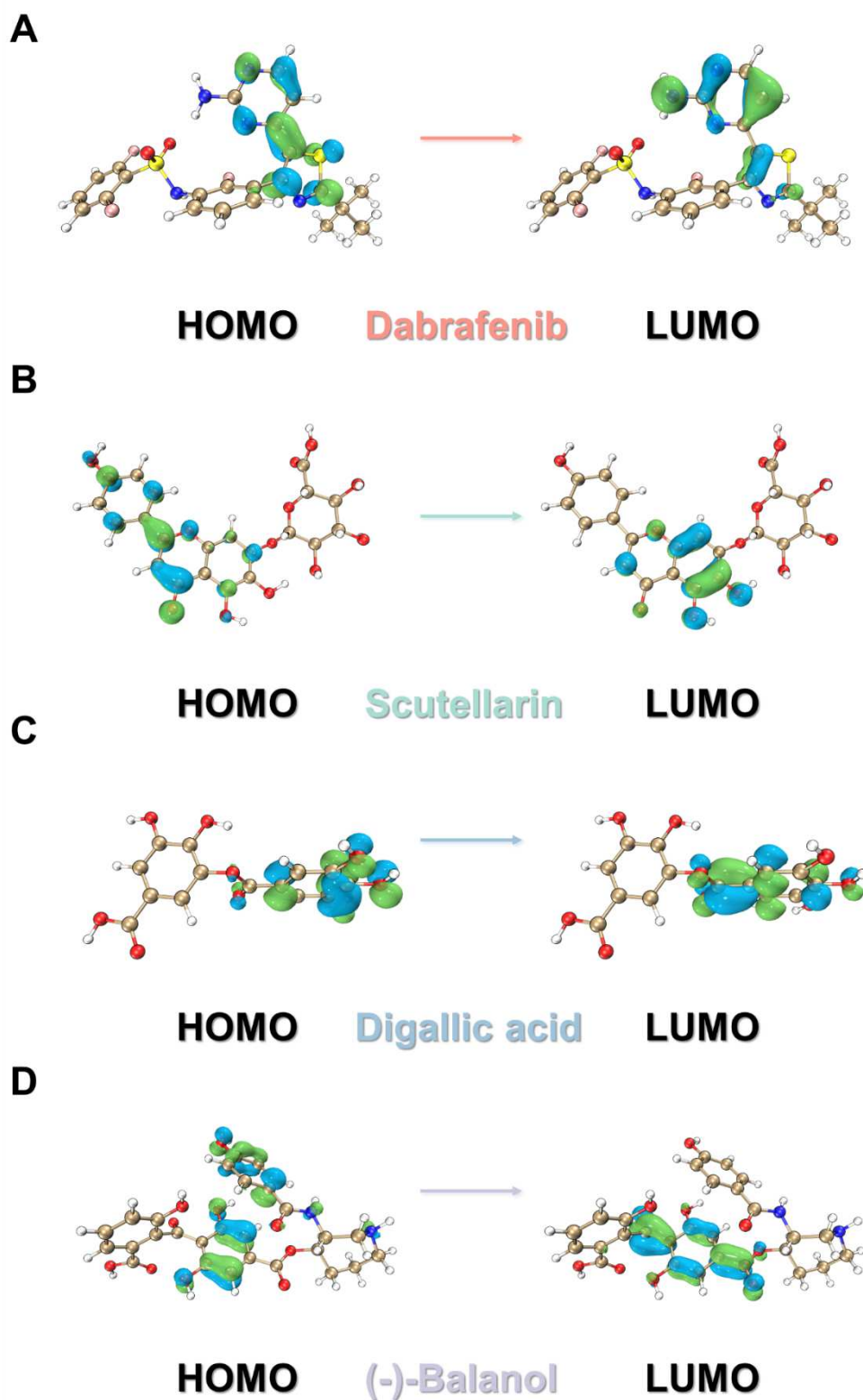
Fig. 6 Frontier orbital analysis. Plots of HOMO to LUMO transition of (A) dabrafenib, (B) scutellarin, (C) digallic acid, and (D) (-)-balanol. The positive and negative phases of electron density are illustrated in green and blue color, respectively.
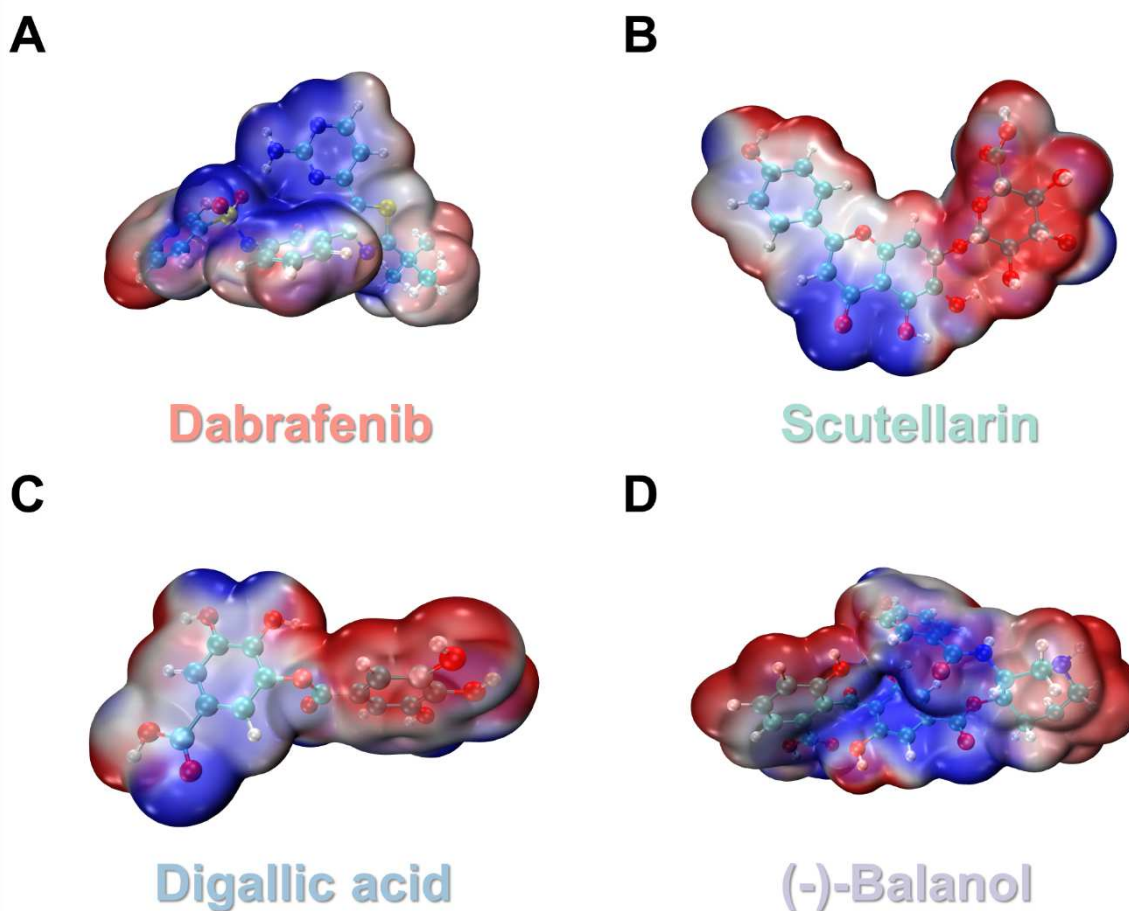
Fig. 7 Molecular electrostatic potential (MEP) plots of (A) dabrafenib, (B) scutellarin, (C) digallic acid, and (D) (-)-balanol. The most positive and negative potential region are shown in blue and red color, respectively.

Molecular dynamics simulation

Relative to molecular docking, molecular dynamics simulations, albeit more computationally demanding, offer a reliable and precise method to compute the temporal behavior of proteins, and to predict their future positions and momentum. This approach is employed in the exploration of the structure, dynamics, and thermodynamics of biomolecules and their complexes. It yields granular information concerning the fluctuations and conformational modifications observed in docked complexes, including protein-ligand interactions

[57,58]. Consequently, founded on the outcomes of molecular docking, molecular dynamics simulations spanning 100ns were conducted on four complexes to assess the stability of protein-ligand binding.

Root mean square deviation (RMSD)

The RMSD values of the complexes reveal conformational alterations relative to the initial structural simulation, serving as a tool to assess the stability and convergence of the simulation process [59]. For all four complexes studied, their RMSD variations remained within acceptable limits [60]. This finding suggests that the triad of natural products and dabrafenib established relatively stable structural interactions with the NEK7 protein. Fluctuations observed in the protein backbone during the simulation could be indicative of minor conformational shifts in NEK7 in the solution (refer to **Fig. 8A**). Specifically, the RMSD of the scutellarin-NEK7 complex (depicted in green) demonstrated a trend towards stabilization post 45 ns, stabilizing around 0.25 nm. Meanwhile, the digallic acid-NEK7 complex (illustrated in blue) exhibited a stable RMSD of 0.22 nm at 75 ns. The (-)-balanol-NEK7 complex (marked in purple) witnessed an overall stabilization following an initial period of acceptable fluctuations, with the RMSD stabilizing at around 0.20 nm post 45 ns. Notably, the dabrafenib-NEK7 complex (denoted in red) displayed minor backbone fluctuations between 55-70 ns, with RMSD peaking at approximately 0.35 nm. This observation suggests potential minor changes in the overall protein conformation, which finally achieved stability post 75 ns and sustained at approximately 0.23 nm until the simulation's conclusion.

Root mean square fluctuation (RMSF)

RMSF serves to expose fluctuations in the average position of protein residues throughout a simulation, thereby facilitating the investigation of the complex system's flexibility and binding effects within the active site [59]. Typically, regions exhibiting minimal fluctuations within the complex suggest a well-structured area with limited deformation. **Fig. 8B** depicts the comparable dynamic fluctuation behaviors across all four systems. Notably, in comparison with the dabrafenib-NEK7 complex, the lower RMSF values associated with the residues related to the active pocket in the dynamic trajectory denote equal stability in the interactions of the three natural products with the NEK7 protein. Consequently, these natural products emerge as potential NEK7 inhibitors.
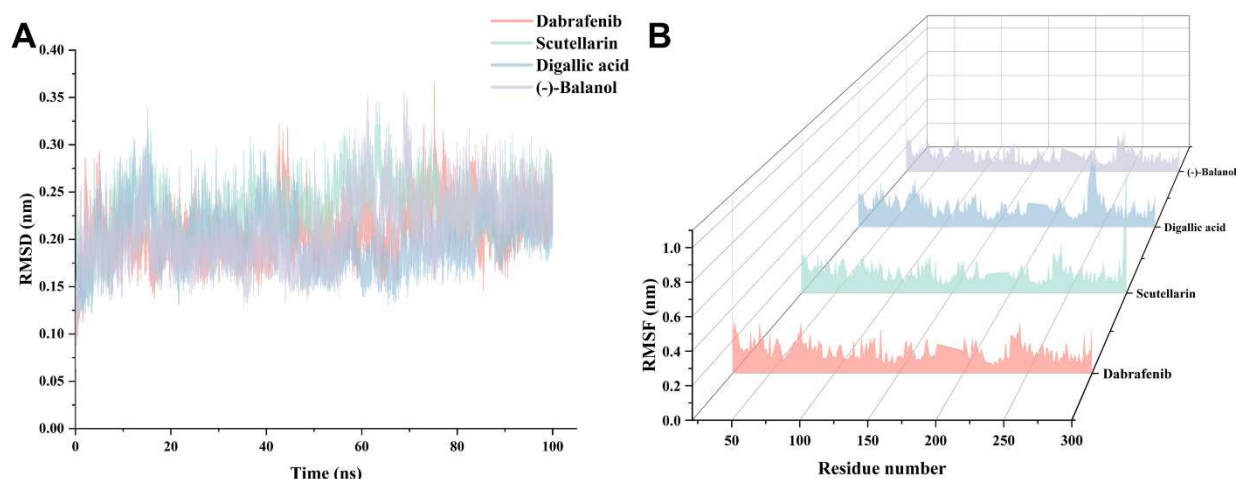

Fig. 8 MD trajectory analysis of reference dabrafenib and hit natural molecules complexed NEK7 protein. (A) RMSD of backbone atoms of NEK7. (B) RMSF.

Radius of gyration (Rg)

The Rg is a crucial parameter in delineating the outcomes of molecular dynamics simulations [61]. It provides an assessment of a protein's compactness, where a lower Rg signifies a more compact structure in the protein-ligand complex throughout the simulation

process, thereby denoting enhanced complex stability. As depicted in **Fig. 9A**, the Rg fluctuations for complexes formed by three natural products and dabrafenib with NEK7 are outlined. The simulated Rg for these selected natural compounds, including dabrafenib, ranged from 1.95 to 2.10 nm, demonstrating a steady state over the 100 ns dynamic trajectory. This suggests that the structural integrity of these molecules remained unaffected upon binding. Consequently, the close packing post-ligand binding leads to the formation of a stable protein complex.

Hydrogen bond (H-bond)

Hydrogen bonding significantly contributes to the binding strength between a ligand and a protein among various interaction methods. To examine the stability of the complex, the complete protein-ligand simulation trajectory is utilized to compute the mean quantity of hydrogen bonds within the complex [62]. The hydrogen bonding patterns of three identified natural compounds and dabrafenib in association with NEK7 are illustrated across the full simulation period, as indicated in **Fig. 9B**. The average hydrogen bond count calculated in the dabrafenib-NEK7, scutellarin-NEK7, digallic acid-NEK7, and (-)-balanol-NEK7 complexes are 0.719, 2.863, 3.291, and 5.227, respectively. Despite minor increases or decreases in the number of protein-ligand hydrogen bonds during the simulation, the three natural products formed, on average, more hydrogen bonds with NEK7 than dabrafenib did. This indicates that the robust binding ability of the natural products with NEK7 may be attributed to hydrogen bonding, aligning with the outcomes of the molecular docking process.

Fig. 9 MD trajectory analysis of reference dabrafenib and hit natural
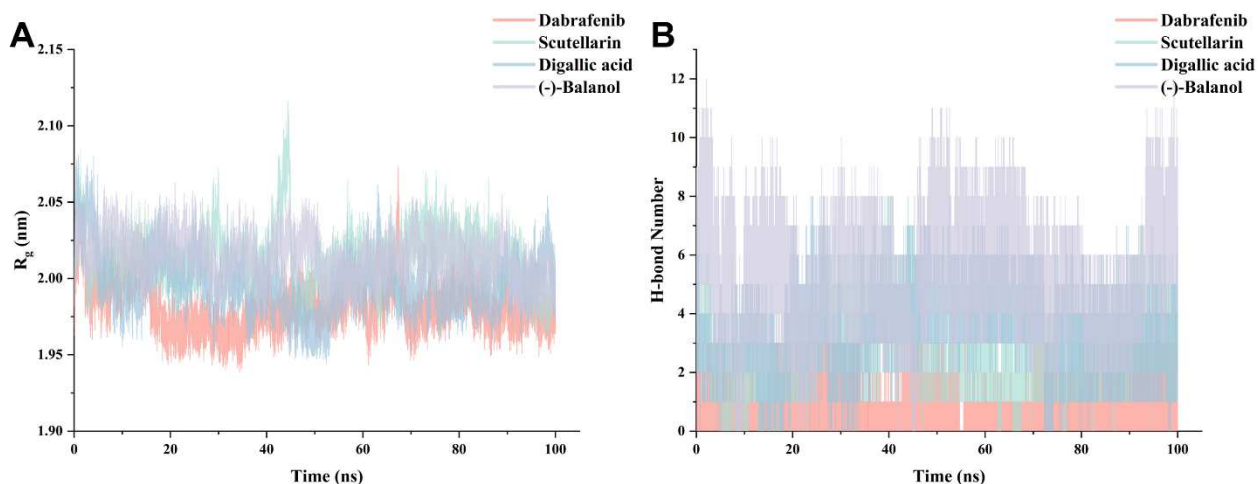
molecules complexed NEK7 protein. (A) Rg. (B) H-bond.

Free energy landscape (FEL)

FEL analysis is utilized to investigate the conformational distribution and stability of protein-ligand complex structures, inferred from the simulation trajectory. The complex stability is gauged by the minimal relative energy where lower free energy corresponds to heightened conformational stability [63]. Areas of lower energy are depicted in darker shades of blue. In this study, a free energy contour map has been formulated for the systems involving kinase NEK7 and four distinct ligands. The Gibbs Free Energy Landscape is derived from principal components serving as reaction coordinates, illustrated in **Fig. 10**. Throughout the simulation, the various accessible conformational states of the four complexes (NEK7-dabrafenib, NEK7-scutellarin, NEK7-digallic acid, and NEK7-(-)-balanol) can be delineated on the free energy landscape, accompanied by two principal components, PC1 and PC2. As depicted in Fig 17, each of the four complexes exhibits one or more distinct basins of global energy minima, each corresponding to their conformational states. The dabrafenib-NEK7 system shows considerable conformational alterations, as evidenced by the broad and dispersed basin on the FEL, thereby underlining the instability

of this complex. Compared to other complexes, the conformations of scutellarin, digallic acid, and (-)-balanol with NEK7 are more compact and centralized on the FEL, suggesting these ligands bind closely with NEK7, thereby adopting stable conformations.
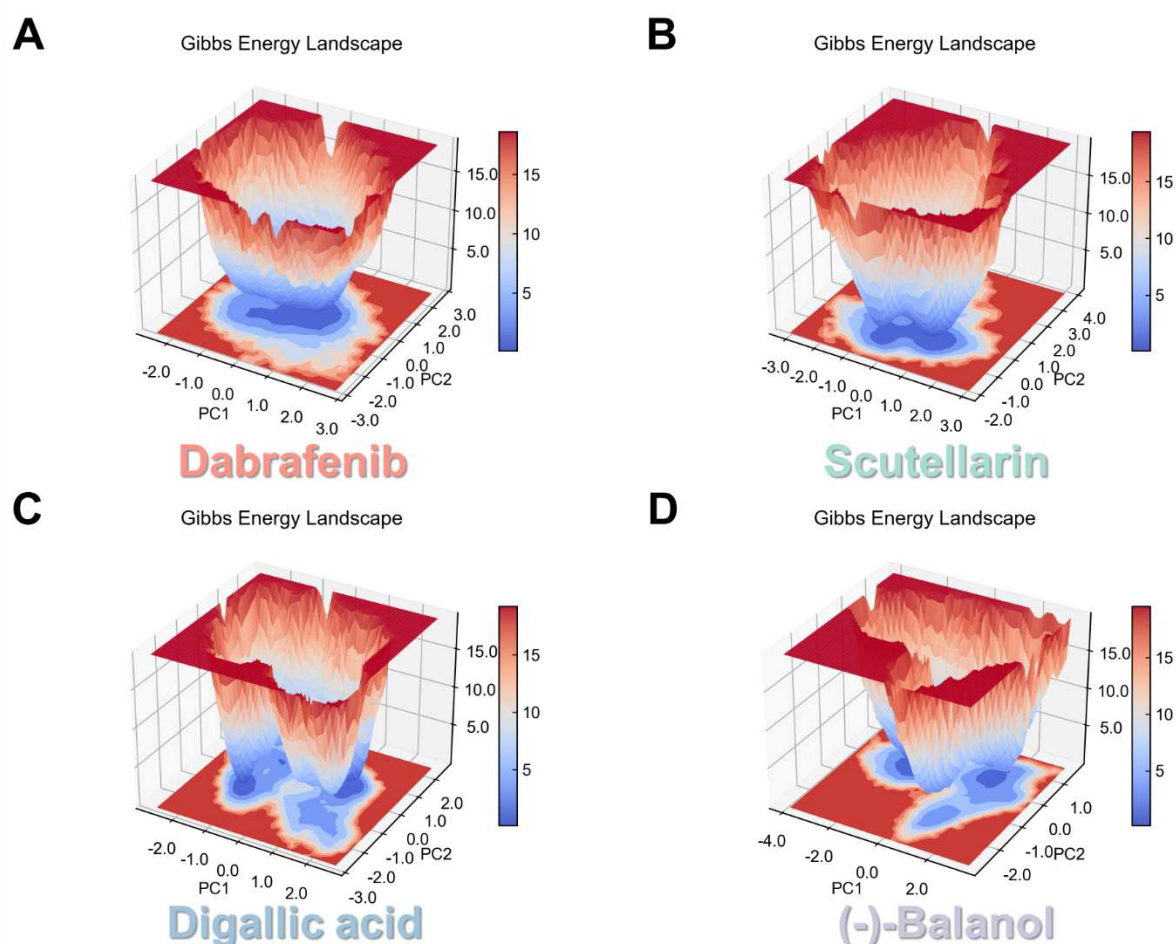

Fig. 10 PCA based FEL analysis. The Gibbs free energy plot was created based on the top principal components. (A) dabrafenib, (B) scutellarin, (C) digallic acid, and (D) (-)-balanol. The Gibbs free energy value (kcal/mol) range is given as color distribution scale.

Vector movements

We further employ Porcupine analysis, grounded in Principal Component Analysis (PCA), to scrutinize the fundamental protein movements vital for biological function [64]. MD simulations

combined with PCA-informed FEL analysis facilitate an expansive exploration of the conformational dynamics of protein-ligand complexes. The Porcupine plot identifies the dominant features of movement, revealing the direction and magnitude of selected eigenvectors for every backbone atom (**Fig. 11**). Within the plot, cones symbolize the movement direction, and their length denotes the amplitude of the motion. The regions with residue indices 11-21, 88-95, 138-145, 200-209, 226-231, 280-296, 327-335, and 348-355 exhibit the most noticeable basic motions of the backbone residues, mirroring the RMSF of NEK7. Observations reveal a lesser amplitude of motion in the residues of scutellarin-NEK7, digallic acid-NEK7, and (-)-balanol-NEK7 complexes than in other complexes, with (-)-balanol showing the minimal amplitude. Loop movements predominate in all systems, which validates our simulations that the stability of scutellarin-NEK7, digallic acid-NEK7, and (-)-balanol-NEK7 complexes surpasses that of the dabrafenib-NEK7 complex.
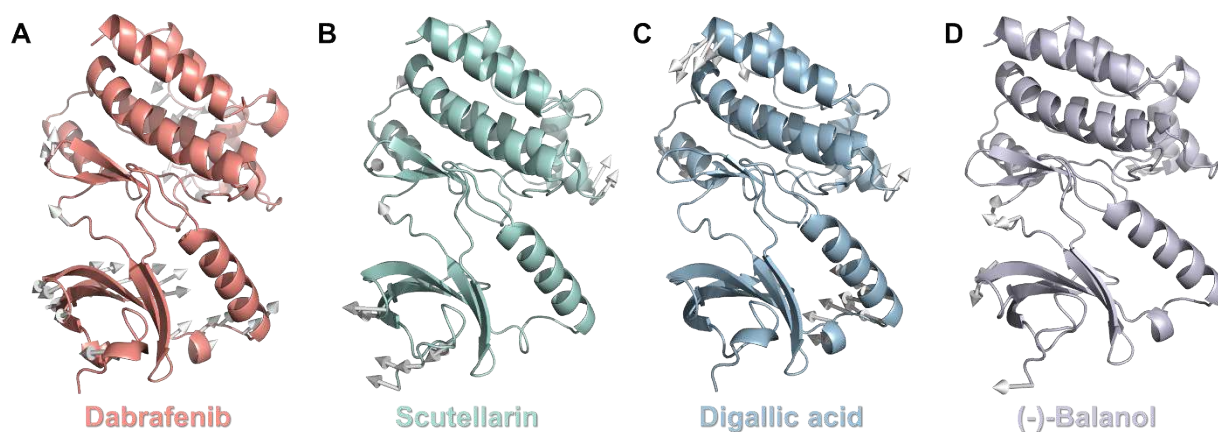

Fig. 11 PCA based porcupine analysis. The porcupine plots representing the principal motions exhibited by the backbone residues of NEK7 complexed with (A) dabrafenib, (B) scutellarin, (C) digallic acid, and (D) (-)-balanol.

Dynamic cross-correlation matrices analysis (DCCM)

A DCCM analysis was implemented to examine the correlated movements of structural domains, thereby stabilizing and confirming the MD trajectories following the ligand interaction of Mur enzymes [65]. The dynamic cross-correlation diagram highlighted the protein's residual fluctuations, indicative of the positive and negative correlations between residue displacements throughout the simulation. The NEK7 enzyme complex, in combination with hit natural products and dabrafenib, was evaluated for positive, negative, and non-correlated movements. The color-coding scheme used to denote correlation strength represented positive correlations in blue and negative correlations in red. **Fig. 12** provides a visual representation of the correlation diagrams, showcasing the interactions between the compound and structural domains during the simulation process that subsequently impact the stability of protein-ligand complexes. Although four types of complexes exhibited correlated and anti-correlated movements, the three natural molecules forming complexes with NEK7 demonstrated superior stability compared to dabrafenib, as their residues displayed less extreme positive and negative correlated movements.
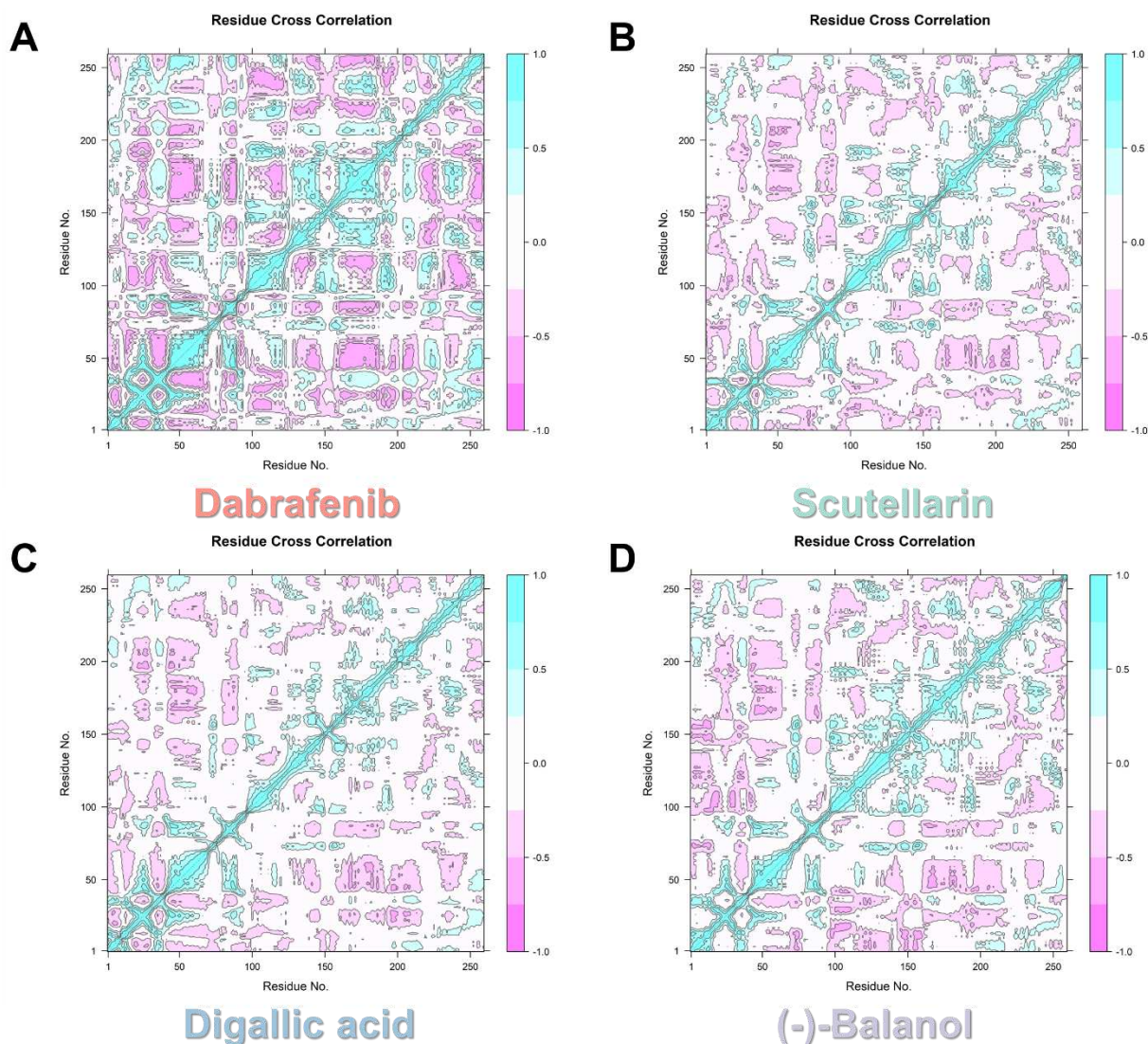
Fig. 12 Dynamic cross-correlation matrix analysis for the backbone residues of NEK7 complexed with (A) dabrafenib, (B) scutellarin, (C) digallic acid, and (D) (-)-balanol.

Secondary structure profile analysis

Structural discrepancies contribute to differences in protein stability [66]. We employed the DSSP module in GROMACS to explore alterations in secondary structural (SS) elements' patterns (α-Helix, β-Sheet, β-Bridge, and Turn) post-ligand binding during simulation, affirming their conformational behavior and folding mechanisms. **Fig. 13** delineates the secondary structural elements'

distribution following complex formation between NEK7 and the target molecules. The DSSP analysis implies that the secondary structural elements in the NEK7-target molecule complexes predominantly preserve as unbroken coils and invariant α-Helix and β-Sheet, with scarce evidence of twisted, turned, or β-Bridge conformations (see **Fig. S2**). Additionally, we discerned a notable trend in the dynamic trajectory: the structural domain formulated by residues 35-40 presented as a coil in the NEK7-dabrafenib complex, whereas in the other three natural product-NEK7 complexes, these structures were more orderly. This observation potentially signals enhanced stability for the natural molecule-NEK7 complexes during the simulation.
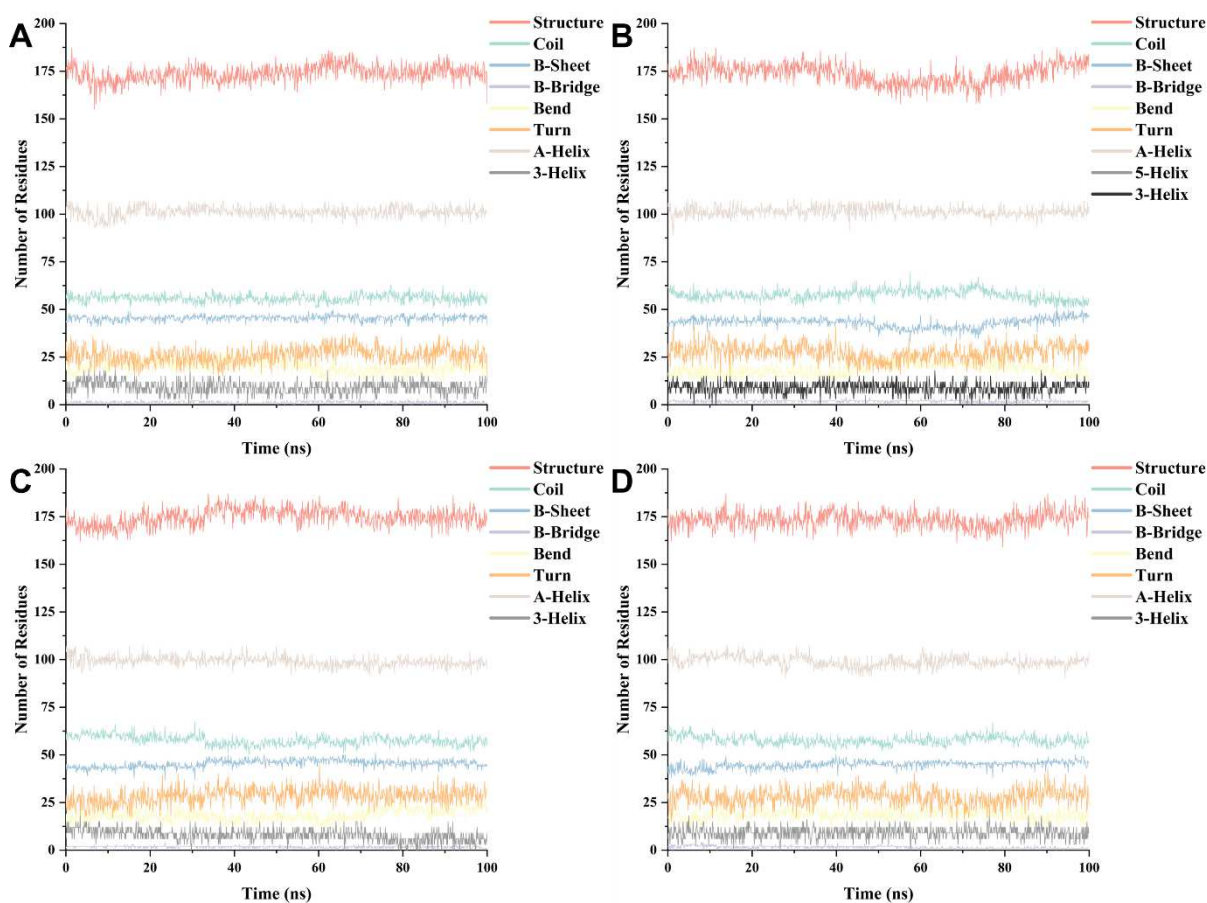

Fig. 13 Secondary structure analysis of (A) dabrafenib, (B) scutellarin, (C) digallic acid, and (D) (-)-balanol. Structure = α-Helix +

β-Sheet + β-Bridge + Turn.

Molecular mechanics Poisson-Boltzmann surface area (MM/PBSA)

To validate and delve into the simulation study findings, we performed calculations of binding free energy, predicting the average binding free energy for protein-ligand complexes [67]. This enabled us to understand better the energy contributions of residues interacting within the binding free energy curve. Generally, a lower binding energy correlates with increased system stability. **Table S1** details the binding energy parameters, encompassing Van der Waals, electrostatic, polar solvent, nonpolar solvent, total gas-phase free energy, total solvation free energy, and total binding energy. The computations revealed that the binding free energies for scutellarin, digallic acid, and (-)-balanol are -35.1397, -40.7140, and -43.8438 kcal/mol, respectively. The hit compounds' binding free energy is significantly lower than that of dabrafenib (**Fig. 14**), implying stronger binding of these compounds to NEK7 than dabrafenib's binding to NEK7. This suggests that these compounds might have potent inhibitory impacts on NEK7.
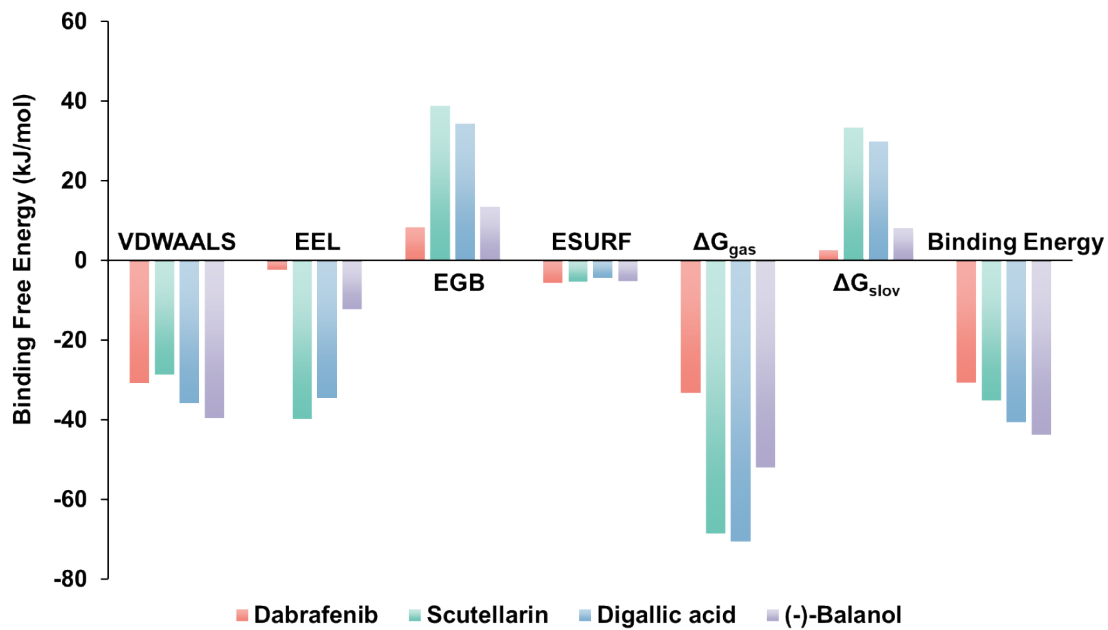
Fig. 14 Calculation of binding free energy using MM/PBSA (kcal/mol).

Among all energy components of protein-ligand complexes, the Van der Waals forces emerge as the principal interaction. Notably, electrostatics also significantly contributes to the system's stability. Conversely, the polar solvation energy, being positive, adversely affects the binding energy. This effect is especially pronounced in the three natural products, which possess greater polar solvation energies than dabrafenib. While the nonpolar solvation energy's importance is less pronounced, its negative value implies a favorable contribution to the binding energy.

Based on the MD simulation results and binding free energy, we executed energy decomposition on amino acid residues and analyzed individual residue contributions. Overall, the key residues' energy of the hit natural products is lesser than that of dabrafenib. Specifically, residues Ile 20, Val 28, Ile 75, Leu91, Glu 92, Leu 93, Ala94, Asp95, Lys 143, Phe 148, Asp 159, Leu 160, and Thr 161 significantly influence the binding effect (see in **Fig. 15**). Among these, residues Ile 20, Val 28, Ile 75, Leu 93, Ala 94, Lys 143, Phe 148, Leu 160, and Thr 161 facilitate compound binding most effectively, whereas residues Glu 92 and Asp 95 are unfavorable for compound binding

Residues	Dabrafenib	Scutellarin	Digallic acid	(-)-Balanol
ILE 20	-1.53264	-1.64151	-1.63729	-2.48237
SER 26	-0.04036	-0.21287	-0.26096	-0.0279
VAL 28	-0.97694	-1.32364	-1.5425	-0.94898
ALA 41	-0.33400	-0.16495	-0.37882	-0.45975
LYS 43	-0.23996	-0.54291	-0.30875	-0.26752
ILE 75	-0.26138	-0.10593	-0.3537	-1.35470
LEU 91	-0.55529	-0.21326	-0.54407	-0.86318
GLU 92	-0.18205	0.072207	-0.19166	-0.64672
LEU 93	-0.73908	-0.36564	-0.70913	-2.32992
ALA 94	-0.57584	-0.14103	-0.52506	-1.33410
ASP 95	-0.36826	0.123585	0.061048	-0.44337
LYS 143	-1.74106	-0.21603	-0.24419	-0.18774
PHE 148	-0.14025	-1.16963	-1.97361	-3.89306
ASP 159	-0.25868	-0.07866	-0.18804	-0.53492
LEU 160	-0.17521	-0.15283	-0.33970	-1.21953
THR 161	-1.09641	-0.48281	-0.55523	-0.03246

to NEK7.

Fig. 15 MM/PBSA per residue energy contribution to the binding energy for the complexes formed by the compounds dabrafenib, scutellarin, digallic acid, and (-)-balanol. (kcal/mol)

Conclusion

In this investigation, natural products were selected for potential inhibitor development from three distinct databases, with the selection process rooted in the structural analysis of NEK7 and using dabrafenib as a comparative reference. We applied a systematic, structure-based virtual screening method for NEK7, leading to the identification of three novel target molecules with promising pharmacodynamics: scutellarin, digallic acid, and (-)-balanol. Molecular docking results highlighted a stable conformation with superior binding energy and affinity, while all three natural products exhibited robust molecular interactions and elevated docking scores. Comprehensive ADME/T studies followed, assessing the compounds' toxicity, drug-likeness, and metabolic properties. It's worth noting that these natural compounds might require additional modification to enhance certain ADME/T characteristics. Furthermore, we employed Density Functional Theory to calculate FMO and MEP, thus verifying the compounds' chemical reactivity and stability. Both scutellarin and (-)-balanol demonstrated greater chemical reactivity. The conclusions drawn from the molecular docking were substantiated by molecular dynamics simulations. RMSD trajectory analysis, along with RMSF, Rg, H-bond, FEL, Vector movements, DCCM, and SS analyses, confirmed a higher degree of stability in the complexes formed by the natural products with NEK7 as compared to that of dabrafenib-NEK7. MM/PBSA binding analysis ratified the effective binding of the natural molecule candidates at the binding site, resulting in the formation of stable NEK7 complexes. These findings suggest the potential inhibitory capacity of these natural products against NEK7; nevertheless, we advocate for additional preclinical, in vitro, and controlled studies to authenticate

these prospective natural products. Overall, the implemented computational approach holds promise in the early stages of rational design for innovative and low-toxicity NEK7 inhibitors in cancer therapy.

Declarations

Ethical approval

This is not applicable.

Ethics declarations

This work did not involve any human subjects.

Consent to participate

This article does not have any studies with human participants or animals, clinical trial registration, or plant reproducibility performed by any author.

Consent for publication

All authors have approved the paper and agree with its publication.

Competing interests

The authors declare no competing interests.

Author contributions

Heng Zhang: data curation, formal analysis, methodology, resources, software, writing—original draft, writing—review editing. Chenhong Lu: investigation and methodology. Qilong Yao: MD simulation, docking analysis, manuscript review, and editing. Qingcai Jiao: conceptualization, methodology, project administration, supervision, validation, visualization, writing — review and editing.

References

1. Nguyen K, Boehling J, Tran MN, Cheng T, Rivera A, Collins-Burow BM, Lee SB, Drewry DH, Burow ME. NEK Family Review and Correlations with Patient Survival Outcomes in Various Cancer Types. *Cancers* 2023;**15**:2067.

2. van de Kooij B, Creixell P, van Vlimmeren A, Joughin BA, Miller CJ, Haider N, Simpson CD, Linding R, Stambolic V, Turk BE, Yaffe MB. Comprehensive substrate specificity profiling of the human Nek kinome reveals unexpected signaling outputs. *eLife* 2019;**8**:e44635. doi: 10.7554/eLife.44635

3. Yamamoto Y, Chino H, Tsukamoto S, Ode KL, Ueda HR, Mizushima N. NEK9 regulates primary cilia formation by acting as a selective autophagy adaptor for MYH9/myosin IIA. *Nat Commun* 2021;**12**:3292. doi: 10.1038/s41467-021-23599-7

4. Takatani S, Verger S, Okamoto T, Takahashi T, Hamant O, Motose H. Microtubule Response to Tensile Stress Is Curbed by NEK6 to Buffer Growth Variation in the Arabidopsis Hypocotyl. *Current Biology* 2020;**30**:1491-1503.e1492. doi: https://doi.org/10.1016/j.cub.2020.02.024

5. Au FKC, Hau BKT, Qi RZ. Nek2-mediated GAS2L1 phosphorylation and centrosome-linker disassembly induce centrosome disjunction. *Journal of Cell Biology* 2020;**219** doi: 10.1083/jcb.201909094

6. Gorry R, Brennan K, Lavin PTM, Sheridan R, Mc Gee MM. Phosphorylation of the prolyl isomerase Cyclophilin A regulates its localisation and release from the centrosome during mitosis. *Cell Cycle* 2023;**22**:951-966. doi: 10.1080/15384101.2023.2167430

7. Liu G, Chen X, Wang Q, Yuan L. NEK7: a potential therapy target for NLRP3-related diseases. *BioScience Trends* 2020;**14**:74-82. doi: 10.5582/bst.2020.01029

8. Müller M, Eghbalian R, Boeckel J-N, Frese KS, Haas J, Kayvanpour E, Sedaghat-Hamedani F, Lackner MK, Tugrul OF, Ruppert T, Tappu R, Martins Bordalo D, Kneuer JM, Piekarek A, Herch S, Schudy S, Keller A, Grammes N, Bischof C, Klinke A, Cardoso-Moreira M, Kaessmann H, Katus HA, Frey N, Steinmetz LM, Meder B. NIMA-related kinase 9 regulates the phosphorylation of the essential myosin light chain in the heart. *Nat Commun* 2022;**13**:6209. doi: 10.1038/s41467-022-33658-2

9. Yan Z, Da Q, Li Z, Lin Q, Yi J, Su Y, Yu G, Ren Q, Liu X, Lin Z, Qu J, Yin W, Liu J. Inhibition of NEK7 Suppressed Hepatocellular Carcinoma Progression by Mediating Cancer Cell Pyroptosis. *Frontiers in Oncology* 2022;**12** doi: 10.3389/fonc.2022.812655

10. Eisa NH, Jilani Y, Kainth K, Redd P, Lu S, Bougrine O, Abdul Sater H, Patwardhan CA, Shull A, Shi H, Liu K, Elsherbiny NM, Eissa LA, El-Shishtawy MM, Horuzsko A, Bollag R, Maihle N, Roig J, Korkaya H, Cowell JK, Chadli A. The co-chaperone UNC45A is essential for the expression of mitotic kinase NEK7 and tumorigenesis. *J Biol Chem* 2019;**294**:5246-5260. doi: https://doi.org/10.1074/jbc.RA118.006597

11. Kang D, Cho H-S, Toyokawa G, Kogure M, Yamane Y, Iwai Y, Hayami S, Tsunoda T, Field HI, Matsuda K, Neal DE, Ponder BAJ, Maehara Y, Nakamura Y, Hamamoto R. The histone

methyltransferase Wolf–Hirschhorn syndrome candidate 1-like 1 (WHSC1L1) is involved in human carcinogenesis. *Genes, Chromosomes and Cancer* 2013;**52**:126-139. doi: https://doi.org/10.1002/gcc.22012

12. Saloura V, Cho H-S, Kiyotani K, Alachkar H, Zuo Z, Nakakido M, Tsunoda T, Seiwert T, Lingen M, Licht J, Nakamura Y, Hamamoto R. WHSC1 Promotes Oncogenesis through Regulation of NIMA-Related Kinase-7 in Squamous Cell Carcinoma of the Head and Neck. *Molecular Cancer Research* 2015;**13**:293-304. doi: 10.1158/1541-7786.Mcr-14-0292-t

13. Yan Z, Qu J, Li Z, Yi J, Su Y, Lin Q, Yu G, Lin Z, Yin W, Lu F, Liu J. NEK7 Promotes Pancreatic Cancer Progression And Its Expression Is Correlated With Poor Prognosis. *Frontiers in Oncology* 2021;**11** doi: 10.3389/fonc.2021.705797

14. O'Regan L, Barone G, Adib R, Woo CG, Jeong HJ, Richardson EL, Richards MW, Muller PAJ, Collis SJ, Fennell DA, Choi J, Bayliss R, Fry AM. EML4–ALK V3 oncogenic fusion proteins promote microtubule stabilization and accelerated migration through NEK9 and NEK7. *Journal of Cell Science* 2020;**133** doi: 10.1242/jcs.241505

15. Hernandez DF, Cervantes EL, Luna-Vital DA, Mojica L. Food-derived bioactive compounds with anti-aging potential for nutricosmetic and cosmeceutical products. *Critical Reviews in Food Science and Nutrition* 2021;**61**:3740-3755. doi: 10.1080/10408398.2020.1805407

16. Bagherniya M, Mahdavi A, Shokri-Mashhadi N, Banach M, Von Haehling S, Johnston TP, Sahebkar A. The beneficial therapeutic effects of plant-derived natural products for the treatment of sarcopenia. *Journal of Cachexia, Sarcopenia and Muscle* 2022;**13**:2772-2790. doi: https://doi.org/10.1002/jcsm.13057

17. Yu L, Tao J, Zhao Q, Xu C, Zhang Q. Confirmation of potential neuroprotective effects of natural bioactive compounds from traditional medicinal herbs in cerebral ischemia treatment. *JIN* 2020;**19**:373-384. doi: 10.31083/j.jin.2020.02.63

18. Rampogu S, Lee G, Kulkarni AM, Kim D, Yoon S, Kim MO, Lee KW. Computational Approaches to Discover Novel Natural Compounds for SARS-CoV-2 Therapeutics. *ChemistryOpen* 2021;**10**:593-599. doi: https://doi.org/10.1002/open.202000332

19. van Santen JA, Jacob G, Singh AL, Aniebok V, Balunas MJ, Bunsko D, Neto FC, Castaño-Espriu L, Chang C, Clark TN, Cleary Little JL, Delgadillo DA, Dorrestein PC, Duncan KR, Egan JM, Galey MM, Haeckl FPJ, Hua A, Hughes AH, Iskakova D, Khadilkar A, Lee J-H, Lee S, LeGrow N, Liu DY, Macho JM, McCaughey CS, Medema MH, Neupane RP, O'Donnell TJ, Paula JS, Sanchez LM, Shaikh AF, Soldatou S, Terlouw BR, Tran TA, Valentine M, van der Hooft JJJ, Vo DA, Wang M, Wilson D, Zink KE, Linington RG. The Natural Products Atlas: An Open Access Knowledge Base for Microbial Natural Products Discovery. *ACS Central Science* 2019;**5**:1824-1833. doi: 10.1021/acscentsci.9b00806

20. van Santen JA, Poynton EF, Iskakova D, McMann E, Alsup Tyler A, Clark TN, Fergusson CH, Fewer DP, Hughes AH, McCadden CA, Parra J, Soldatou S, Rudolf JD, Janssen EM-L, Duncan KR, Linington RG. The Natural Products Atlas 2.0: a database of microbially-derived natural products. *Nucleic Acids Res* 2021;**50**:D1317-D1323. doi: 10.1093/nar/gkab941

21. Irwin JJ, Tang KG, Young J, Dandarchuluun C, Wong BR, Khurelbaatar M, Moroz YS, Mayfield J, Sayle RA. ZINC20—A Free Ultralarge-Scale Chemical Database for Ligand Discovery.

Journal of Chemical Information and Modeling 2020;**60**:6065-6073. doi: 10.1021/acs.jcim.0c00675

22. Sterling T, Irwin JJ. ZINC 15 – Ligand Discovery for Everyone. *Journal of Chemical Information and Modeling* 2015;**55**:2324-2337. doi: 10.1021/acs.jcim.5b00559

23. Xue Q, Liu X, Russell P, Li J, Pan W, Fu J, Zhang A. Evaluation of the binding performance of flavonoids to estrogen receptor alpha by Autodock, Autodock Vina and Surflex-Dock. *Ecotoxicology and Environmental Safety* 2022;**233**:113323. doi: https://doi.org/10.1016/j.ecoenv.2022.113323

24. Abdulwahab MK, Tan KH, Dzulkeflee R, Leong KH, Heh CH, Ariffin A. In-silico Studies of the Antiproliferative Activity of New Anilinoquinazoline Derivatives Against NSCLC Cells. *Journal of Molecular Structure* 2021;**1228**:129786. doi: https://doi.org/10.1016/j.molstruc.2020.129786

25. Perike N, Edigi PK, Nirmala G, Thumma V, Bujji S, Naikal PS. Synthesis, Anticancer Activity and Molecular Docking Studies of Hybrid Molecules Containing Indole-Thiazolidinedione-Triazole Moieties. *ChemistrySelect* 2022;**7**:e202203778. doi: https://doi.org/10.1002/slct.202203778

26. Ramadhan DSF, Siharis F, Abdurrahman S, Isrul M, Fakih TM. In silico analysis of marine natural product from sponge (Clathria Sp.) for their activity as inhibitor of SARS-CoV-2 Main Protease. *Journal of Biomolecular Structure and Dynamics* 2022;**40**:11526-11532. doi: 10.1080/07391102.2021.1959405

27. Hammoud MM, Khattab M, Abdel-Motaal M, Van der Eycken J, Alnajjar R, Abulkhair HS, Al-Karmalawy AA. Synthesis, structural characterization, DFT calculations, molecular docking, and molecular dynamics simulations of a novel ferrocene derivative to unravel its potential antitumor activity. *Journal of*

Biomolecular Structure and Dynamics 2023;**41**:5199-5216. doi: 10.1080/07391102.2022.2082533

28. Jablonský M, Štekláč M, Majová V, Gall M, Matúška J, Pitoňák M, Bučinský L. Molecular docking and machine learning affinity prediction of compounds identified upon softwood bark extraction to the main protease of the SARS-CoV-2 virus. *Biophysical Chemistry* 2022;**288**:106854. doi: https://doi.org/10.1016/j.bpc.2022.106854

29. Aziz M, Ejaz SA, Rehman HM, Alsubaie AS, Mahmoud KH, Siddique F, Al-Buriahi MS, Alrowaili ZA. Identification of NEK7 inhibitors: structure based virtual screening, molecular docking, density functional theory calculations and molecular dynamics simulations. *Journal of Biomolecular Structure and Dynamics* 2022:1-15. doi: 10.1080/07391102.2022.2113563

30. K. P SH, K. A AR, Medammal Z, Thayyil MS, Babu TD. Theoretical insights into the radical scavenging activity of glipizide: DFT and molecular docking studies. *Free Radical Research* 2022;**56**:53-62. doi: 10.1080/10715762.2022.2034803

31. Yadav JK, Yadav P, Singh VK, Agarwal A. Molecular docking and density functional theory studies of potent 1,3-disubstituted-9H-pyrido[3,4-b]indoles antifilarial compounds. *Structural Chemistry* 2021;**32**:1925-1947. doi: 10.1007/s11224-021-01772-4

32. Vázquez-Jiménez LK, Juárez-Saldivar A, Gómez-Escobedo R, Delgado-Maldonado T, Méndez-Álvarez D, Palos I, Bandyopadhyay D, Gaona-Lopez C, Ortiz-Pérez E, Nogueda-Torres B, Ramírez-Moreno E, Rivera G. Ligand-Based Virtual Screening and Molecular Docking of Benzimidazoles as Potential Inhibitors of Triosephosphate Isomerase Identified New

Trypanocidal Agents. *International Journal of Molecular Sciences* 2022;**23**:10047.

33. Karthick R, Velraj G, Pachamuthu MP, Karthikeyan S. Synthesis, spectroscopic, DFT, and molecular docking studies on 1,4-dihydropyridine derivative compounds: a combined experimental and theoretical study. *Journal of Molecular Modeling* 2021;**28**:5. doi: 10.1007/s00894-021-04939-2

34. Fu L, Zhao L, Liang M, Ran K, Fu J, Qiu H, Li F, Shu M. Identification of potential CAMKK2 inhibitors based on virtual screening and molecular dynamics simulation. *Molecular Simulation* 2023;**49**:27-35. doi: 10.1080/08927022.2022.2123945

35. Murad HAS, Alqurashi TMA, Hussien MA. Interactions of selected cardiovascular active natural compounds with CXCR4 and CXCR7 receptors: a molecular docking, molecular dynamics, and pharmacokinetic/toxicity prediction study. *BMC Complementary Medicine and Therapies* 2022;**22**:35. doi: 10.1186/s12906-021-03488-8

36. Xiong G, Wu Z, Yi J, Fu L, Yang Z, Hsieh C, Yin M, Zeng X, Wu C, Lu A, Chen X, Hou T, Cao D. ADMETlab 2.0: an integrated online platform for accurate and comprehensive predictions of ADMET properties. *Nucleic Acids Research* 2021;**49**:W5-W14. doi: 10.1093/nar/gkab255

37. Zhang D, Wang Z, Li J, Zhu J. Exploring the possible molecular targeting mechanism of Saussurea involucrata in the treatment of COVID-19 based on bioinformatics and network pharmacology. *Computers in Biology and Medicine* 2022;**146**:105549. doi: https://doi.org/10.1016/j.compbiomed.2022.105549

38. Che Omar MT. Data analysis of molecular dynamics simulation trajectories of β-sitosterol, sonidegib and cholesterol in

smoothened protein with the CHARMM36 force field. *Data in Brief* 2020;**33**:106350. doi: https://doi.org/10.1016/j.dib.2020.106350

39. Sapay N, Tieleman DP. Combination of the CHARMM27 force field with united-atom lipid force fields. *Journal of Computational Chemistry* 2011;**32**:1400-1410. doi: https://doi.org/10.1002/jcc.21726

40. Stroet M, Caron B, Visscher KM, Geerke DP, Malde AK, Mark AE. Automated Topology Builder Version 3.0: Prediction of Solvation Free Enthalpies in Water and Hexane. *Journal of Chemical Theory and Computation* 2018;**14**:5834-5845. doi: 10.1021/acs.jctc.8b00768

41. King E, Aitchison E, Li H, Luo R. Recent Developments in Free Energy Calculations for Drug Discovery. *Frontiers in Molecular Biosciences* 2021;**8** doi: 10.3389/fmolb.2021.712085

42. Poli G, Granchi C, Rizzolio F, Tuccinardi T. Application of MM-PBSA Methods in Virtual Screening. *Molecules* 2020;**25**:1971.

43. Samanta R, Pradhan KK, Sen D, Kar S, Ghosh M. Structure-based drug design-guided identification of estrogen receptor binders. *Molecular Diversity* 2023 doi: 10.1007/s11030-023-10657-z

44. Vesaghhamedani S, Mazloumi Kiapey SS, Gowhari Shabgah A, Amiresmaili S, Jahanara A, Oveisee M, Shekarchi A, Gheibihayat SM, Jadidi-Niaragh F, Gholizadeh Navashenaq J. From traditional medicine to modern oncology: Scutellarin, a promising natural compound in cancer treatment. *Progress in Biophysics and Molecular Biology* 2023;**180-181**:19-27. doi: https://doi.org/10.1016/j.pbiomolbio.2023.04.006

45. Alfonso EE, Troche R, Deng Z, Annamalai T, Chapagain P, Tse-Dinh Y-C, Leng F. Potent Inhibition of Bacterial DNA Gyrase by

Digallic Acid and Other Gallate Derivatives. *ChemMedChem* 2022;**17**:e202200301. doi: https://doi.org/10.1002/cmdc.202200301

46. Bhouri W, Boubaker J, Skandrani I, Ghedira K, Chekir Ghedira L. Investigation of the apoptotic way induced by digallic acid in human lymphoblastoid TK6 cells. *Cancer Cell International* 2012;**12**:26. doi: 10.1186/1475-2867-12-26

47. Hardianto A, Yusuf M, Liu F, Ranganathan S. Exploration of charge states of balanol analogues acting as ATP-competitive inhibitors in kinases. *BMC Bioinformatics* 2017;**18**:572. doi: 10.1186/s12859-017-1955-7

48. Nogara PA, Saraiva RdA, Caeran Bueno D, Lissner LJ, Lenz Dalla Corte C, Braga MM, Rosemberg DB, Rocha JBT. Virtual Screening of Acetylcholinesterase Inhibitors Using the Lipinski's Rule of Five and ZINC Databank. *BioMed Research International* 2015;**2015**:870389. doi: 10.1155/2015/870389

49. O' Donovan DH, De Fusco C, Kuhnke L, Reichel A. Trends in Molecular Properties, Bioavailability, and Permeability across the Bayer Compound Collection. *Journal of Medicinal Chemistry* 2023;**66**:2347-2360. doi: 10.1021/acs.jmedchem.2c01577

50. Hu L, Wang J, Zhao X, Cai D. Mechanism of saikogenin G against major depressive disorder determined by network pharmacology. *Medicine* 2022;**101**:e30193. doi: 10.1097/md.0000000000030193

51. El Aissouq A, Bouachrine M, Ouammou A, Khalil F. Homology modeling, virtual screening, molecular docking, molecular dynamic (MD) simulation, and ADMET approaches for identification of natural anti-Parkinson agents targeting MAO-B protein. *Neuroscience Letters* 2022;**786**:136803. doi: https://doi.org/10.1016/j.neulet.2022.136803

52. Roy R, Sk MF, Jonniya NA, Poddar S, Kar P. Finding potent inhibitors against SARS-CoV-2 main protease through virtual screening, ADMET, and molecular dynamics simulation studies. *Journal of Biomolecular Structure and Dynamics* 2022;**40**:6556-6568. doi: 10.1080/07391102.2021.1897680

53. Almazroo OA, Miah MK, Venkataramanan R. Drug Metabolism in the Liver. *Clinics in Liver Disease* 2017;**21**:1-20. doi: https://doi.org/10.1016/j.cld.2016.08.001

54. Zhou S, Zhao F-L, Wang S-H, Wang Y-R, Hong Y, Zhou Q, Geng P-W, Luo Q-F, Cai J-P, Dai D-P. Assessments of CYP-inhibition-based drug–drug interaction between vonoprazan and poziotinib in vitro and in vivo. *Pharmaceutical Biology* 2023;**61**:356-361. doi: 10.1080/13880209.2023.2173253

55. Islam MR, Osman OI, Hassan WMI. Identifying novel therapeutic inhibitors to target FMS-like tyrosine kinase-3 (FLT3) against acute myeloid leukemia: a molecular docking, molecular dynamics, and DFT study. *Journal of Biomolecular Structure and Dynamics* 2023:1-19. doi: 10.1080/07391102.2023.2192798

56. Su A, Zhang X, Zhang C, Ding D, Yang Y-F, Wang K, She Y-B. Deep transfer learning for predicting frontier orbital energies of organic materials using small data and its application to porphyrin photocatalysts. *Physical Chemistry Chemical Physics* 2023;**25**:10536-10549. doi: 10.1039/D3CP00917C

57. Arshad R, Khan MA, Mutahir S, Hussain S, Al-Hazmi GH, Refat MS. DFT, Molecular Docking and ADME Studies of Thiazolidinones as Tyrosinase Inhibitors. *Polycyclic Aromatic Compounds* 2022:1-16. doi: 10.1080/10406638.2022.2124286

58. Ashok AK, Gnanasekaran TS, Santosh Kumar HS, Srikanth K, Prakash N, Gollapalli P. High-throughput screening and

molecular dynamics simulations of natural products targeting LuxS/AI-2 system as a novel antibacterial strategy for antibiotic resistance in Helicobacter pylori. *Journal of Biomolecular Structure and Dynamics* 2023:1-16. doi: 10.1080/07391102.2023.2210674

59. Ashiru MA, Ogunyemi SO, Temionu OR, Ajibare AC, Cicero-Mfon NC, Ihekuna OA, Jagun MO, Abdulmumin L, Adisa QK, Asibor YE, Okorie CJ, Lawal MO, Babalola MO, Abdulrasaq IT, Salau LB, Olatunji IO, Bankole MA, Daud AB, Adeyemi AO. Identification of EGFR inhibitors as potential agents for cancer therapy: pharmacophore-based modeling, molecular docking, and molecular dynamics investigations. *Journal of Molecular Modeling* 2023;**29**:128. doi: 10.1007/s00894-023-05531-6

60. Guterres H, Park S-J, Jiang W, Im W. Ligand-Binding-Site Refinement to Generate Reliable Holo Protein Structure Conformations from Apo Structures. *Journal of Chemical Information and Modeling* 2021;**61**:535-546. doi: 10.1021/acs.jcim.0c01354

61. Singh A, Mishra A. Molecular modelling study to discover novel JAK2 signaling pathway inhibitor. *Journal of Biomolecular Structure and Dynamics* 2022:1-12. doi: 10.1080/07391102.2022.2097314

62. Chen J, Yu X, Chen Q, Wu Q, He Q. Screening and mechanisms of novel angiotensin-I-converting enzyme inhibitory peptides from rabbit meat proteins: A combined in silico and in vitro study. *Food Chemistry* 2022;**370**:131070. doi: https://doi.org/10.1016/j.foodchem.2021.131070

63. Almeleebia TM, Ahamad S, Ahmad I, Alshehri A, Alkhathami AG, Alshahrani MY, Asiri MA, Saeed A, Siddiqui JA, Yadav DK, Saeed M. Identification of PARP12 Inhibitors By Virtual Screening and

Molecular Dynamics Simulations. *Frontiers in Pharmacology* 2022;**13** doi: 10.3389/fphar.2022.847499

64. Kumar D T, Shaikh N, Kumar S U, Doss C GP, Zayed H. Structure-Based Virtual Screening to Identify Novel Potential Compound as an Alternative to Remdesivir to Overcome the RdRp Protein Mutations in SARS-CoV-2. *Frontiers in Molecular Biosciences* 2021;**8** doi: 10.3389/fmolb.2021.645216

65. Shafie A, Khan S, Zehra, Mohammad T, Anjum F, Hasan GM, Yadav DK, Hassan MI. Identification of Phytoconstituents as Potent Inhibitors of Casein Kinase-1 Alpha Using Virtual Screening and Molecular Dynamics Simulations. *Pharmaceutics* 2021;**13**:2157.

66. Markthaler D, Fleck M, Stankiewicz B, Hansen N. Exploring the Effect of Enhanced Sampling on Protein Stability Prediction. *Journal of Chemical Theory and Computation* 2022;**18**:2569-2583. doi: 10.1021/acs.jctc.1c01012

67. Borkotoky S, Banerjee M, Modi GP, Dubey VK. Identification of high affinity and low molecular alternatives of boceprevir against SARS-CoV-2 main protease: A virtual screening approach. *Chemical Physics Letters* 2021;**770**:138446. doi: https://doi.org/10.1016/j.cplett.2021.138446

Figures

Figure 9

Figure 10

Figure 11

Figure 12

Figure 13

Figure 14

Figure 15

Figure 16

Figure 17

Figure 18

Figure 19

Figure 20

Figure 21

Figure 22

Figure 23

Supplementary Files

This is a list of supplementary files associated with this preprint. Click to download.

- Table3.docx
- Table4.docx
- Table7.docx
- Table.docx
- Table6.docx
- Table1.docx
- Table5.docx
- Table2.docx
- SupplementaryMaterials.docx